REPORT DOCUMENTATION PAGE

1. REPORT DATE (DD-MM-YYYY)	2. REPORT TYPE	3. DATES COVERED (From - To)
02/02/2016	Technical Report for year one	3/10/2015-2/2/16

4. TITLE AND SUBTITLE
The exploitation of the electric contributions in infrared power generation

5a. CONTRACT NUMBER

5b. GRANT NUMBER
N00014-15-1-2158

5c. PROGRAM ELEMENT NUMBER

6. AUTHOR(S)
Scarel, Giovanna
Utter, Brian, C

5d. PROJECT NUMBER
1000000586

5e. TASK NUMBER

5f. WORK UNIT NUMBER

7. PERFORMING ORGANIZATION NAME(S) AND ADDRESS(ES)
James Madison University
800 South Main Street
Harrisonburg, Virginia 22807-0002

8. PERFORMING ORGANIZATION REPORT NUMBER

9. SPONSORING/MONITORING AGENCY NAME(S) AND ADDRESS(ES)
Office of Naval Research
875 N. Randolph Street Suite 1425
Arlington, Virginia 22203-1995

10. SPONSOR/MONITOR'S ACRONYM(S)
ONR

11. SPONSOR/MONITOR'S REPORT NUMBER(S)

12. DISTRIBUTION/AVAILABILITY STATEMENT
Approved for public release; distribution is unlimited.

13. SUPPLEMENTARY NOTES

14. ABSTRACT This project studies the basic processes involved in the interaction of infrared radiation with matter and, in this effort, establishes a method to harvest infrared radiation and transform it into usable energy. We have identified an electrical contribution to the energy transfer from the infrared radiation to the device we use to harvest it. This device behaves as a capacitor, and we found a way to triplicate the voltage generated by the device when exposed to the infrared radiation. This significant increase can be obtained by placing two devices in series and covering the surface of the device facing the infrared radiation to tape, which modifies the capacitance of the device. We plan on modeling the interaction of the infrared radiation with our device using the conjugated variable-based approach. We also plan on studying the current produced by the device to increase efficiency in power generation. We are also looking into other alternative device designs to fabricate nano- and macro-power generation device. Seven undergraduate students were involved in the research and the research inspired an approach to Thermodynamics and Statistical Mechanics related to the conjugated variable-based approach. We plan on outlining the view in a textbook.

15. SUBJECT TERMS
Keywords: infrared radiation, radiation harvesting, renewable and sustainable energy source

16. SECURITY CLASSIFICATION OF:			17. LIMITATION OF ABSTRACT	18. NUMBER OF PAGES	19a. NAME OF RESPONSIBLE PERSON
a. REPORT	b. ABSTRACT	c. THIS PAGE			Giovanna Scarel, Principal Investigator
			UU	11	19b. TELEPHONE NUMBER (Include area code) (540) 568-8857

20160208000

Office of Naval Research (ONR) – The sea warfare and weapons department (Code 33)

JMU Technical point of contact:
Dr. Giovanna Scarel (Principal Investigator - PI) – Dr. Brian C. Utter (Co-PI)
JMU, Department of Physics and Astronomy
901 Carrier Drive, MSC 4502, PhCh Building, Harrisonburg, VA 22807, USA
Phone: +1 540 568-8857, Fax: +1 540 568-2800
e-mail address: scarelgx@jmu.edu
                     utterbc@jmu.edu

JMU Administrative/business contact:
Mr. John D. Hulvey
Director, Sponsored Programs Administration and Accounting
JMU, MSC 5728, 1031 Harrison Street, JMAC 6, Suite 26, Harrisonburg, Virginia 22807, USA
Phone: +1 540 568-3725, Fax: +1 540 568-6240
e-mail address: hulveyjd@jmu.edu

ONR Technical point of contact:
Program officer (Code:331): Mr. Lynn J. Petersen, One Liberty Center, 875 N. Randolph St., Arlington, VA 22203-1995, USA
Phone: +1 703 696-8181
e-mail address: lynn.j.petersen@navy.mil

ONR Administrative/business contact:
Mr. Rob Notman, Syntek Technologies Contractor Support to ONR Code 331
Phone: +1 703-254-4578
e-mail address: rnotman@syntek.org

Note: the final Report for this Project will be provided in February 2017.

Fig. 1. Schematic of the PG device hit by IR radiation. The figure shows the sequence of insulating and semiconducting layers (AlO and Bi_2Te_3) acting as dielectrics. The metallic (Cu) layers behave as electrodes [4].

OBJECTIVE:

The electrodynamic mechanisms of blackbody emission of infrared (IR) radiation from matter are well known, as testified by the prolific literature existing in the field and covering scientific aspects and applications [1-3]. The reversed process, however, i.e. the interaction of IR radiation
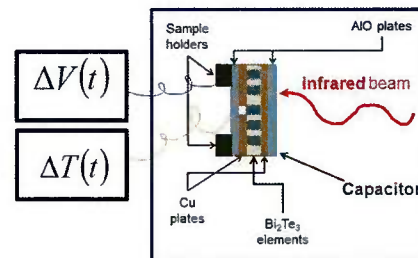
1

with matter, is still obscure. This Project aims at unveiling the basic mechanisms involved in the IR radiation-matter interaction, and outlining the possible applications related to harvesting IR radiation as a sustainable and renewable source of energy. These two goals are achieved by illuminating a power generator (PG) device, shown in Fig. 1, with IR radiation, and studying the voltage difference ΔV, the current I, the power $\Delta V*I$, and temperature difference ΔT produced as a function of time t upon starting the illumination. This procedure is *IR power generation*. In addition, this Project also aims at (i) training undergraduate students in energy-related science and technology relevant for the U.S. Navy, (ii) disseminating knowledge derived from IR power generation to general and scientific audience, and (iii) developing knowledge relevant for a course in Thermodynamics and Statistical Mechanics.

Fig. 2. (a) Amplitude of jump in voltage, $\Delta(\Delta V)$, immediately after starting the illumination with IR radiation of a PG device in geometries named A and T and covered or not with tape. (b) $\Delta(\Delta V)$ obtained when a PG device is activated by a 100 Ω resistor placed in contact with the active face of the device in geometries A and T, and covered or not with tape [4].

Scientific and technological objectives. In **Year-1** we discovered the existence of an electric and an entropic contribution in the energy transfer from IR radiation to matter through the PG device [4]. Additionally, we found that, with the electric contribution, the PG device has a *capacitor-type* behavior, whereas it has a *thermoelectric-type* behavior with the entropic contribution. We also started examining the effects on the voltage difference $\Delta V(t)$ of (i) colored tape covering the illuminated face of the PG device (Fig. 2), (ii) angle of incidence θ of the IR radiation with respect to the PG device (Fig. 3), (iii) in-series coupling of two PG devices (Fig. 3), (iv) variable laser power [with Marc Currie at the Naval Research Laboratory (NRL) and Oleksandr Kokhan (JMU)] (Fig. 4), (v) nano-scale architecture of the PG device (Figs. 5 and 6) with active element consisting of a thin film of variable resistance fabricated via atomic layer deposition (ALD) by Virginia D. Wheeler at NRL. We disseminated the knowledge we acquired through the **Workshop** on "*Infrared radiation, Thermoelectricity and Chaos*" which took place on June 17, 2015 at JMU. The Workshop was funded by the ONR Award # N000141410378. In **Year-2** we will complete the objectives of Year-1. In addition, we will (i) develop a macro-PG device with Boris Feygelson at NRL, (ii) study the current I(t) produced when the PG device is illuminated by IR radiation, and (iii) model the behavior in time t of the variables at play in IR power generation adopting the *conjugated-variable based approach* to capture the mechanism triggering the switch in behavior of the
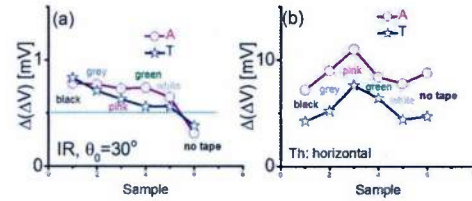

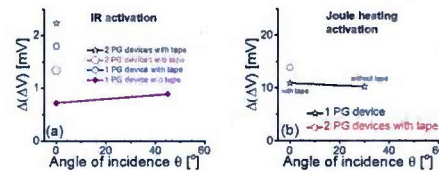**Fig. 3.** (a) Amplitude of jump in voltage, $\Delta(\Delta V)$, immediately after starting the illumination with IR radiation of a PG device in various settings (tape or in-series coupling) versus angle of incidence θ. (b) $\Delta(\Delta V)$ obtained when a PG device is activated by a 100 Ω resistor placed in contact with the active face of the device in various device geometries.

PG device from *capacitor-type* to *thermoelectric-type*, and vice-versa.

Educational objective. In **Year-1**, (i) 7 undergraduate students participated in research and dissemination activities related to this Project, and (ii) we shared knowledge and awareness on IR power generation to a general audience [5], and the broader scientific community [6-12]. In **Year-2** we plan on disseminating our results in venues such as AVS 63rd International Symposium, 94th Annual Meeting of the Virginia Academy of Science, 2016 Undergraduate Research Symposium in Physics (JMU), 2016 Summer REU Research Symposium (JMU), and, possibly, SPIE Optics and Photonics Nanoscience and Engineering Conference; San Diego (CA), August 30-September 1, 2016. In

Fig. 4. Amplitude of jump in voltage, $\Delta(\Delta V)$, and temperature, $\Delta(\Delta T)$, immediately after starting the illumination with an IR laser of a PG device versus average power for (a) CW laser, and (b) pulsed laser. Panel (c) zooms into the low power region of panel (b).

addition, we plan on developing an innovative approach to Thermodynamics and Statistical Mechanics using a *conjugated-variable based approach*. We showed that this concept is useful in recognizing the electric and the entropic contributions in IR power generation [4], and propose that it might be useful also for other physical phenomena. We plan on drafting a textbook in Thermodynamics and Statistical Mechanics possibly also with additional funding.

Significance and Future Naval Relevance: The low frequency and low power radiation studied in this Project is important for fundamental studies and also for applications on ships, satellites, cars, personal backpacks, and, more generally, where non-dangerous energy is needed at all hours of the day, independent of weather conditions. Full understanding of power $\Delta V * I$ generation, and designing robust devices (nano-PG or macro-PG devices) are important objectives to implement the concept of IR power generation and move it into applications. The importance of our studies lies also in that the method of harvesting IR radiation using a PG device could be extended to other electromagnetic radiation. Broadening the spectrum of the usable electromagnetic radiation would greatly contribute to the exploitation of the electric contribution for an efficient sustainable and renewable source of energy available to humankind.

TECHNICAL REPORT.
Scientific achievements.

(i) **Decoupling of the electric and entropic contributions in IR power generation**. We discovered that energy transfers from IR radiation into matter (e.g. the illuminated surface of the PG device) affects the couples of conjugated variables consisting of charge q and voltage V, on one hand, and entropy Σ and temperature T, on the other. The q-V couple generates the electric contribution and dominates when IR radiation activates the PG device [4]. This contribution imparts on the PG device a *capacitor-type* behavior, and is sensitive on how the insulating and conducting layers alternate in the PG device (Fig. 1). The Σ-T couple generates the entropic contribution, and dominates when Joule heating, due to an electrical resistance, activates the PG device [4]. This contribution imparts on the PG device a *thermoelectric-type* behavior obeying the Seebeck effect: $\Delta V(t) = S * \Delta T(t)$, where S is the Seebeck coefficient. We have yet to explain
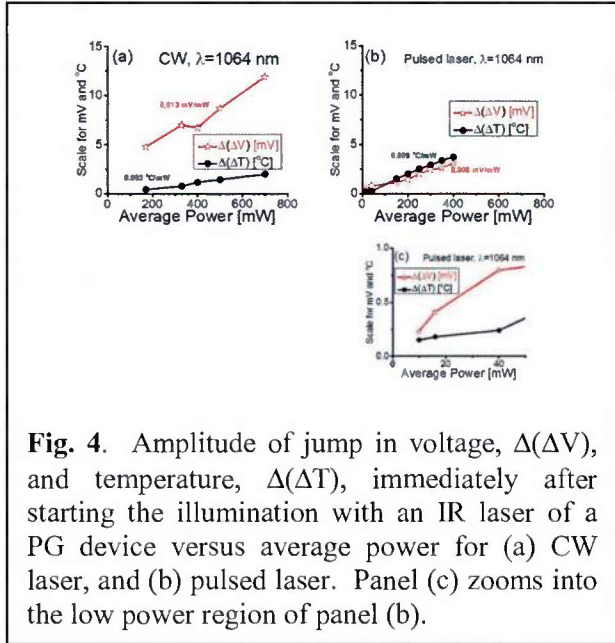
what switches the PG device's behavior from *capacitor-type* to *thermoelectric-type*, and vice-versa, and plan on using the *conjugated-variable based approach* in this effort. Relevant couples of conjugated variables will be charge q and voltage V, and entropy Σ and temperature T. Here, $q=\sigma(z,t)$*surface area, where $\sigma(z,t)$ is surface charge density.

(ii) **Effect of colored tape on the production of voltage $\Delta V(t)$ in IR power generation**. We discovered that when the electric contribution is at play in the interaction between IR radiation and matter in a PG device, the amplitude of the voltage jump $\Delta(\Delta V)$ achieved upon starting the illumination can be increased at least twice by simply placing tape on the face of the PG device hit by IR radiation. The finding is illustrated in Fig. 2a [4], and is not detected when the entropic

Fig. 5. Schematic of a nano-PG device illuminated by IR radiation. The ALD film connects electrically the "hot" and "cold" faces of the device made of copper plates.

contribution dominates, as can be seen in Fig. 2b. This result (a) decouples the electric from the entropic contribution, and (b) suggests that tape can modify the capacitance C of the PG device. Thus, we need to investigate on the role of C in switching the PG device behavior's from
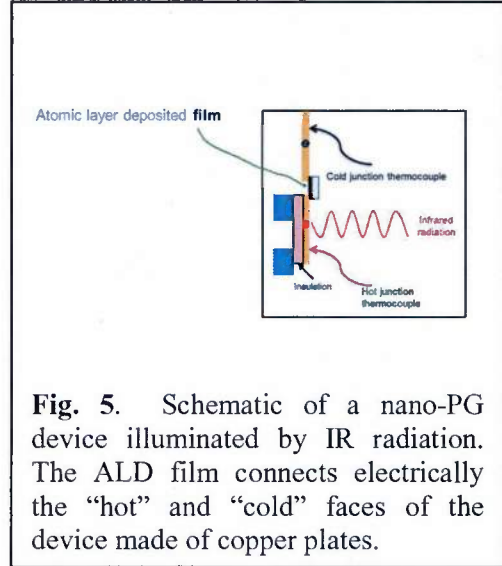
$$\Delta(\Delta V)\{Tape\}/\Delta(\Delta V) = 2.5$$

capacitor-type to *thermoelectric-type*, and vice-versa.

(iii) **Effect of angle of incidence θ on the production of $\Delta V(t)$ in IR power generation**. We found that the amplitude of the voltage jump $\Delta(\Delta V)$ slightly increases with the angle of incidence θ of the IR radiation on the PG device. The phenomenon is illustrated in Fig. 3a. We did not observe a clear dependence on θ of $\Delta(\Delta V)$ when the PG device is activated by Joule heating, as shown in Fig. 3b. With will need to collect more data to better characterize this phenomenon, and, possibly, use it to decouple the electric from the entropic contribution in IR

$$\Delta(\Delta V)\{45°\}/\Delta(\Delta V) = 1.2$$

power generation.

(iv) **Effect of in-series coupling of two PG devices on the production of $\Delta V(t)$ in IR power generation**. We coupled two PG devices in series, and found that the amplitude of the voltage jump $\Delta(\Delta V(t))$ increases after starting the illumination with IR radiation, as can be seen in Fig. 3a. The amplitude can **increase up to three times** when tape is used in addition to in-series coupling. We did not observe a clear increase in $\Delta(\Delta V)$ when the PG devices are activated by Joule heating, as shown in Fig. 3b. Also in this case we will need to collect more data to

exploit this finding and use it to decouple the electric from the entropic contribution in IR power

$$\Delta(\Delta V)\{2PG+Tape\}/\Delta(\Delta V)=3.1$$

generation.

$$\Delta(\Delta V)\{2PG+Tape\}/\Delta(\Delta V)\{2PG\}=1.6$$

Fig. 6. Amplitude of jump in voltage, $\Delta(\Delta V)$, and temperature, $\Delta(\Delta T)$, immediately after starting the activation of a nano-PG device with IR radiation and a 100 Ω resistor placed in contact with the active face of the device.

(v) **Effect of variable laser power on the production of $\Delta V(t)$ in IR power generation**. In collaboration with Marc Currie at NRL and Oleksnadr Kokhan at JMU, we are testing the effects of IR radiation's power on PG devices. We are using monochromatic lasers at wavelength λ=1064 nm with range of average power from 5 to 700 mW. With continuous wave (CW) lasers, the power remains constant throughout the duration of the illumination. With pulsed lasers, the power changes from a minimum to a peak value over a well-defined pulse duration. The peak-power in our experiments spans from the kW to the MW range. Our results with the CW lasers, summarized in Fig. 4a, indicate that the amplitude of the voltage jump $\Delta(\Delta V)$ and of the temperature jump $\Delta(\Delta T)$ increase linearly, however the slope of $\Delta(\Delta V)$ vs. average power is 0.013 mV/mW, one order of magnitude larger than that of $\Delta(\Delta T)$ vs. average power, which is 0.003 °C/mW. We interpret this discrepancy as an effect of the prevalence of the electric contribution, and of its independence from the entropic contribution. On the other hand, our results for the pulsed laser case, summarized in Fig. 4b and 4c, indicate that the amplitudes of $\Delta(\Delta V)$ and $\Delta(\Delta T)$ increase linearly vs. average power and with similar slopes, 0.008 mV/mW and 0.009 °C/mW, respectively. This behavior is consistent with the Seebeck effect, and points out the prevalence of the entropic contribution. From the experimental point of view, we will need to investigate the effects of (i) colored tape, (ii) angle of incidence θ, and (iii) in-series coupling of PG devices illuminated by the lasers to gain further insight on what causes switch of the of PG devices behavior from *capacitor-type* to *thermoelectric-type* when illuminated by CW and pulsed lasers, respectively.

(vi) **Effect of a nano-scale architecture of the PG device with active element consisting of a thin film layer fabricated via ALD with variable resistance**. With the collaboration of Virginia D. Wheeler at NRL we have fabricated thin films of variable resistance to build nano-PG devices as sketched in Fig. 5, and test their response to IR radiation and Joule heating. The thin films so far consist of stacks of conducting (e.g. TiN) and non-conducting (e.g. TiO_2) layers deposited via ALD. This technique enables precise thickness and doping control. The thin film resistance so far spans from about 90 Ω/sq to 67 kΩ/sq. Our results, summarized in Fig. 6, indicate that the illumination of the nano-PG device with IR radiation raises the amplitude of the voltage jump $\Delta(\Delta V)$ with increasing the thin film resistance. This finding is quite unexpected and not yet understood. We plan on exploring whether the observed trend persists at even higher and lower resistances.
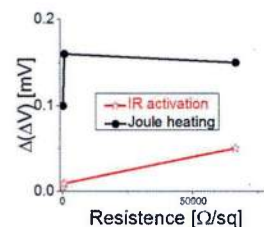
5

(•) **Conclusions**: The current picture of the interaction of IR radiation with matter, achieved through our studies on IR power generation, is as follows. The transfer of energy from IR radiation obeys the laws of conservation and is constrained by the balance between the following couples of conjugated variables active in the process: charge (q) and voltage (V), and entropy (Σ) and temperature (T). When low power IR radiation illuminates a PG device, the electric contribution dominates and dictates a *capacitor-type* behavior to the device. In this situation, q and V are related by the capacitance C of the PG device and, by properly engineering C, maximum efficiency can be achieved in harvesting IR radiation. When the power of the IR radiation is increased to the kW range and above, the entropic contribution, related to Σ and T, dominates and dictates a *thermoelectric-type* behavior to the PG device. This situation suppresses voltage production at the advantage of temperature increase. The circumstances of the switch in the PG device behavior must be investigated and might involve an entanglement among the conjugated-variables q-V and Σ-T. These findings are important for harvesting IR radiation as a renewable and sustainable source of energy. The picture on the behavior of the conjugated variables might impact other scenarios: e.g., in biology and medicine the nerve system is viewed as capacitor system which might be affected by low power IR radiation [13, 14] in ways similar to those described in this research.

Educational achievements.

The ***educational* results** achieved are as follows:

(•) ***Student training***: In Summer 2015 three undergraduate students (Justin M. Kaczmar, Graham P. Gearhart and Tara R. Jobin) performed work with the PI and Co-PI. These students were entirely supported by ONR Award # N000141512158. Four other students were involved: Zachary J. Marinelli, Aidan L. Gordon, Brian N. Lang, and Yosyp Schwab. In Fall 2015 Aidan L. Gordon, performed modeling and data analysis work for this Project and received a stipend for it. Supervised by the PI, Co-PI, and technical personnel at JMU, the students assembled the insulated compartment, interfaced the experimental set-up with the electronic data collection system, and finally collected and analyzed the experimental data. The students used the machine shops at JMU, were involved in the intellectual effort of modeling and understanding the data, and presented the results at various venues [8-12]. The student's efforts were rewarded by their inclusion in the list of authors of the publication reporting most of the recent findings [4]. Five students actively participated to the Workshop on "*Infrared radiation, Thermoelectricity and Chaos*" on June 17, 2015 at JMU.

(•) ***Academic outreach***: In Fall 2015, the PI taught the course on Thermodynamics and Statistical Mechanics PHYS 380 at JMU stemming out from the observation that the *conjugated variable-based approach* can (a) broaden the concept of heat, and (b) include the description of several phenomena such as equilibrium, stability, the laws of Thermodynamics, phase equilibrium, specific heat, compressibility, boson and fermion statistics, Maxwell-Boltzman distribution for the momentum of many non-correlated particles, momentum for correlated particles, the law of ideal gases, properties of solids at low temperatures, magnetic properties of materials, continuity equation in fluids and Fick's laws. The PI became convinced that the *conjugated variable-based approach* can also serve as the framework in which to model the research in this Project on IR power generation. The *conjugated variable-based approach* generated a new and original way to design and deliver the lectures in PHYS 380. All the newly developed class material is now in hand-written notes. However the PI thinks that it is worth the effort to draft a textbook based on these notes and will pursue this goal in the future months.

(•) ***Broader outreach***: Two main objectives were achieved:

→ The PI illustrated some of the findings of the research project-ONR Award # N000141512158 in an event organized by the Mount Jackson Rotary Club, Mount Jackson (VA), on August 4, 2015 [5]. Similar events might take place in the near future. The PI's presentation was well received and effective in disseminating the awareness of the U.S. Navy's interest in alternative sustainable energy programs.

→ The PI presented the finding in the project at two international venues [6, 7] focusing on the general aspects of IR power generation [6] and on the potentials of the nano-PG devices [7]. The PI's presentations generated discussions with other researchers (e.g. A. V. Zenkevich, the organizer of the event in Moscow) and created connections with Angela Belcher – MIT in Boston, Leora Peltz – Boeing in Huntington Beach (CA), and Scott Strum – Medical School at Loma Linda University in Loma Linda, CA.

Bibliography.

[1] J. Le Gall, M. Olivier, and J.-J. Greffet, *Experimental and theoretical study of reflection and coherent thermal emission by a SiC grating supporting of a surface –phonon polariton*", Phys. Rev. B **55**, 10105-10114 (1997).

[2] B. Song, A. Fiorino, E. Meyhofer, and P. Reddy, *Near-field radiative thermal transport: From theory to experiment*, AIP Advances **5**, 053503 (2015).

[3] O. D. Miller, S. G. Johnson, A. W. Rodriguez, *Shape-independent limits to near-field radiative heat transfer*, Phys. Rev. Lett. **115**, 204301 (2015).

[4] A. L. Gordon, Y. Schwab, B. N. Lang, G. P. Gearhart, T. R. Jobin, J. M. Kaczmar, Z. J. Marinelli, H. S. Mann, B. C. Utter, and G. Scarel, *Decoupling the electrical and entropic contributions to energy transfer from infrared radiation to a power generator*, World J. Cond. Matter Phys. **5**, 301-318 (2015).

[5] G. Scarel, *Infrared power generation*, Mount Jackson Rotary Club; Mount Jackson (VA), August 4, 2015.

[6] G. Scarel, *Atomic layer deposition for rare earth oxides and thermoelectric thin films*, Atomic layer Deposition: Russia 2015; Moscow (Russian Federation), September 21-23, 2015.

[7] G. Scarel, V. D. Wheeler, H. S. Mann, B. N. Lang, Z. J. Marinelli, and B. C. Utter, *The nano-power generator fabricated with thin atomic layer deposited films*, AVS 62nd International Symposium; San José (CA), October 18-23, 2015.

[8] G. P. Gearhart, B. C. Utter, and G. Scarel, *Tape-influenced infrared and thermal power generation*, 2015 Undergraduate Research Symposium in Physics; JMU; Harrisonburg (VA), March 21, 2015.

[9] A. L. Gordon, B. C. Utter, and G. Scarel, *Determining a mathematical model for a voltage-induced, exclusively temporal soliton*, 93th Annual Meeting of the Virginia Academy of Science; JMU; Harrisonburg (VA), May 21-23, 2015.

[10] T. R. Jobin, J. M. Kaczmar, B. C. Utter, and G. Scarel, *Voltage hyperbolic instablities from infared radiation*, 2015 Summer REU Research Symposium; JMU; Harrisonburg (VA), July 30-31, 2015.

[11] A.L. Gordon, B.C. Utter, and G. Scarel, *Modeling solitons of charge density*, 2015 Summer REU Research Symposium; JMU, Harrisonburg (VA), July 30-31, 2015.

[12] J. M. Kaczmar, T. R. Jobin, B. C. Utter, and G. Scarel, *Correlation between the sinusoidal instability in radiation power and the hyperbolic instability in the voltage in infrared*

power generation, International Symposium on Clusters and Nanomaterials; Richmond (VA), October 26-29, 2015.

[13] C.-P. Richter, S. Rajguru, R. Stafford, and S. R. Stock, *Radiant energy during infrared neural stimulation at the target structure*, Proc. SPIE **8565**, 85655P-. doi: 10.1117/12.2013849 (2013).

[14] D. Eisen, D. Janssen, X. Chen, F.-S. Choa, D. Kotsov, and J. Fan, *Closing a Venus Flytrap with electrical and mid-IR photon stimulations*, Proc. SPIE 8565, 85655I-. doi. 10.1117/12.2005351 (2013).

Publications acknowledging research project-ONR Award # N000141410378.

(1) A. L. Gordon, Y. Schwab, B. N. Lang, G. P. Gearhart, T. R. Jobin, J. M. Kaczmar, Z. J. Marinelli, H. S. Mann, B. C. Utter, and G. Scarel, *Decoupling the electrical and entropic contributions to energy transfer from infrared radiation to a power generator*, World J. Cond. Matter Phys. **5**, 301-318 (2015).

Scientific presentations acknowledging research project-ONR Award # N000141512158.
(•) <u>**PI**</u>:

(1) G. Scarel, *Infrared power generation*, Mount Jackson Rotary Club; Mount Jackson (VA), August 4, 2015.

(2) G. Scarel, *Infrared power generation: fundamental understanding, applications and benefits*, Workshop on "*Infrared radiation, Thermoelectricity and Chaos*"; JMU, June 17, 2015.

(3) G. Scarel, *Atomic layer deposition for rare earth oxides and thermoelectric thin films*, Atomic layer Deposition: Russia 2015; Moscow (Russian Federation), September 21-23, 2015.

(4) G. Scarel, V. D. Wheeler, H. S. Mann, B. N. Lang, Z. J. Marinelli, and B. C. Utter, *The nano-power generator fabricated with thin atomic layer deposited films*, AVS 62nd International Symposium; San José (CA), October 18-23, 2015.

(•) <u>**Students**</u>:

(1) G. P. Gearhart, B. C. Utter, and G. Scarel, *Tape-influenced infrared and thermal power generation*, 2015 Undergraduate Research Symposium in Physics; JMU; Harrisonburg (VA), March 21, 2015.

(2) A. L. Gordon, B. C. Utter, and G. Scarel, *Determining a mathematical model for a voltage-induced, exclusively temporal soliton*, 93th Annual Meeting of the Virginia Academy of Science; JMU, Harrisonburg (VA), May 21-23, 2015.

(3) T. R. Jobin, J. M. Kaczmar, B. C. Utter, and G. Scarel, *Voltage hyperbolic instablities from infared radiation*, 2015 Summer REU Research Symposium; JMU, Harrisonburg (VA), July 30-31, 2015.

(4) A.L. Gordon, B.C. Utter, and G. Scarel, *Modeling solitons of charge density*, 2015 Summer REU Research Symposium; JMU, Harrisonburg (VA), July 30-31, 2015.

(5) J. M. Kaczmar, T. R. Jobin, B. C. Utter, and G. Scarel, *Correlation between the sinusoidal instability in radiation power and the hyperbolic instability in the voltage in infrared power generation*, International Symposium on Clusters and Nanomaterials; Richmond (VA), October 26-29, 2015.

THE WORKSHOP "*Infrared radiation, Thermoelectricity and Chaos*".
The Workshop, which took place on June 17, 2015 at JMU, was one of the most important activities of the research project-ONR awards # N000141410378 and N000141512158. The

event was organized by the PI and Co-PI together with Mr. Benjamin T. Delp, Director of the JMU Research Development and Promotion Office. The Workshop featured two international speakers. Prof. Giulio Casati of Italy spoke about *Conservation laws, symmetry breaking and control of the heat current.* Prof. Francisco Javier Gonzalez Contreras of México described *Seebeck nanoantennas for solar energy harvesting.* Three speakers represented the U.S.A. academic world. Prof. Gabriel A. Rincón-Mora of the Georgia Institute of Technology, presented *Microwatt CMOS harvesters.* Prof. Rajeevan Amirtharajah of the University of California at Davis, discussed *Powering systems from ambient energy sources.* Finally, Prof. S. Joseph Poon of the University of Virginia, presented *Practical realization of ZT>1 from the materials perspective.* The business and entrepreneurial world was represented by Dr. Ronald J. Parise of Parise Research Technologies, who introduced *The Nighttime solar cell$^®$: infrared energy to deep space.* Dr. Joseph R. Blandino of the Virginia Military Institute, and Dr. David J. Lawrence of JMU, presented a poster on *Transient response of a thermoelectric generator subjected to spatially non-uniform heating: implications for heat and IR sensing applications.* In her presentation, the Dr. G. Scarel (PI) explained the connection among the words in the Workshop's title (IR radiation, thermoelectricity and chaos) justified the selection of the speakers, and illustrated the current knowledge on IRPG. Mr. Lynn J. Petersen, ONR's Program Officer (Code:331) who funded the awards, participated to the event.

Two posters were presented by JMU Physics students Graham P. Gearhart and Brian N. Lang. Graham presented "*Infrared source and thermoelectric device trends in infrared power generation*", while Brian discussed "*The interaction between current and infrared radiation*". The JMU Physics students Justin M. Kaczmar, Zachary J. Marinelli and Tara R. Jobin joined the event by helping in the logistics, asking questions during the sessions and actively networking.

Dr. Brian C. Utter (Co-PI) and Mr. Lynn J, Petersen (ONR) chaired the morning and the afternoon sessions, respectively. Dr. Yvonne R. Harris, JMU's vice Provost for Research and Scholarship, and Mr. Lynn Petersen opened the event in the morning and addressed the final remarks in the afternoon, respectively.

The Workshop was funded by the ONR award # N000141410378. Additional funding, used to support the logistics, pay the honorarium for Dr. J. R. Blandino and partially that of Prof. F. J. Gonzalez, was provided by the JMU 4-VA Consortium and The JMU Madison Trust—Fostering Innovation and Strategic Philanthropy. The international speakers (Prof. G. Casati and Prof. F. J. Gonzalez) were mainly funded by ONR Global-London (UK).

The Workshop revealed that IR power generation explores a rather unknown topic in a unique experimental setting. Specifically:

(•) **F. J. Gonzalez**: excites a PG device exploiting Joule heating, i.e. an *entropic* contribution, derived from an electric current activated in an antenna by the IR radiation. His research does not explore the direct effects of radiation, i.e. of the *electric* contribution, on voltage output as we do in IR power generation.

(•) **R. J. Parise**: uses IR radiation as a means to carry heat to deep space which, acting as a heat sink, facilitates the creation of a temperature difference in a PG device.

(•) **D. J. Lawrence and J. R. Blandino**: use high power fiber optics to activate a PG device. Their results are above the power range of IR power generation.

(•) **G. Casati**: pointed out that the term "soliton" was improperly used by PI in her presentation, thus underlining that the hyperbolic instability highlighted in the briefing on IR power generation is a new entity.

FINANCIAL REPORT.
Expenditures.
(•) Stipends:
→ **Giovanna Scarel** (PI, Assistant Professor, JMU, Department of Physics and Astronomy), Summer 2015, $ 3,609.00

→ **Brian C. Utter** (Co-PI, Associate Professor, JMU, Department of Physics and Astronomy), Summer 2015, $ 3,915.00

→ **Justin M. Kaczmar** (Undergraduate student, JMU, Department of Physics and Astronomy), May 21 – July 31, 2015, $ 8.50/hour, $ 4,000.00

→ **Graham P. Gearhart** (Undergraduate student, JMU, Department of Physics and Astronomy), May 21 – July 3, 2015, $ 8.50/hour, $ 2,000.00

→ **Tara R. Jobin** (Undergraduate student, JMU, Department of Physics and Astronomy), May 21 – July 3, 2015, $ 8.50/hour, $ 2,000.00

→ **Aidan L. Gordon** (Undergraduate student, JMU, Department of Mathematics and Statistics), Fall 2015, $ 8.50/hour, $ 1,000.00

(•) Taxes:
FICA: $ 1,187.59

(•) Travel:
→ Car rental from JMU for G. Scarel's travel to NRL on August 17-19, 2015: $ 82.42. (Sample preparation with Virginia Wheeler and data collection with Marc Currie).

→ Lodging and food for G. Scarel's travel to NRL on August 17-19, 2015: $ 655.82

(•) Miscellaneous:
→ Bruker HeNe laser module to support IR source in PI's laboratory; November 2015: $ 1,500.00

→ PIKE Technologies Crystal Polishing and Polishing kit Cerium Oxide compound to clean KBr window in IR source compartment in PI's laboratory; December 2015: $ 78.42

→ CDW-Government AME-BE350G APC Back UPS for power support of PI's IR source in sample compartment; December 2015: $ 54.01

(•) Indirect cost:
→ $ 9,173.00

Other support.
(•) 4VA Collaborative Research Project 2014-2015: *"Giving to JMU international visibility in infrared power generation and its link to non-linear phenomena"*. PI: G. Scarel (JMU). Co-PIs: Rosa A. Lukaszew (College of William&Mary) and Brian C. Utter (JMU). (*"Infrared radiation, Thermoelectricity and Chaos"* Workshop support).

(•) JMU – Madison Trust—Fostering Innovation and Strategic Philanthropy - Innovation Grant - 2015, November 14, 2014: *"From JMU to the World: embracing the need of new energy sources"*. (Student support and miscellaneous expenses for the Workshop on*"Infrared radiation, Thermoelectricity and Chaos"* Workshop).

(•) JMU – Department of Physics and Astronomy. (Student, equipment and facility support).

ATTACHMENTS.
1) Presentations (3)
2) Papers (1)

ABSTRACT.

This project studies the basic processes involved in the interaction of infrared radiation with matter and, in this effort, establishes a method to harvest infrared radiation and transform it into usable energy. We have identified an electrical contribution to the energy transfer from the infrared radiation to the device we use to harvest it. This device behaves as a capacitor, and we found a way to triplicate the voltage generated by the device when exposed to the infrared radiation. This significant increase can be obtained by placing two devices in series and covering the surface of the device facing the infrared radiation to tape, which modifies the capacitance of the device. We plan on modeling the interaction of the infrared radiation with our device using the conjugated variable-based approach. We also plan on studying the current produced by the device to increase efficiency in power generation. We are also looking into other alternative device designs to fabricate nano- and macro-power generation device. Seven undergraduate students were involved in the research and the research inspired an approach to Thermodynamics and Statistical Mechanics related to the conjugated variable-based approach. We plan on outlining this view in a textbook.

Keywords: infrared radiation, radiation harvesting, renewable and sustainable energy source

Correlation Between the Sinusoidal Instability in Radiation Power and the Hyperbolic Instability in Voltage in Infrared Power Generation

Justin Michael Kaczmar[1], Tara Rose Jobin[1], Brian C. Utter[1], and Giovanna Scarel[1]
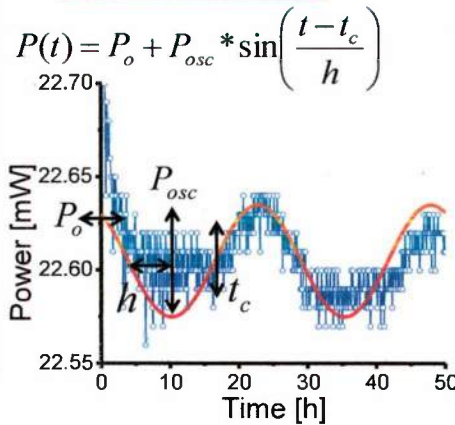
[1]Department of Physics and Astronomy, James Madison University, Harrisonburg VA 22807
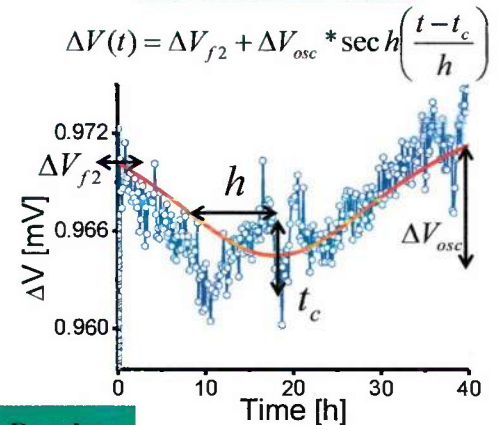
Abstract:

Goal- Looking for methods to harvest alternative sources of energy, specifically infrared, and transform it into usable energy. The advantage in harvesting infrared is its day and night availability. Specifically we are looking at the instability in the power source in comparison to the instability in the resulting voltage the device produces.
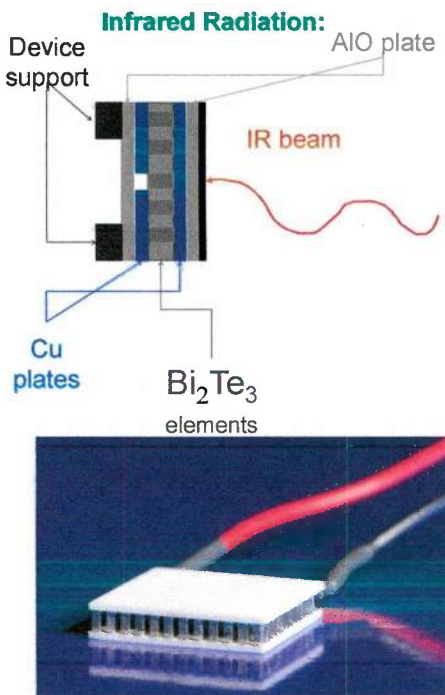
Equation: Power

$$P(t) = P_o + P_{osc} * \sin\left(\frac{t - t_c}{h}\right)$$

Equation: Voltage

$$\Delta V(t) = \Delta V_{f2} + \Delta V_{osc} * \sec h\left(\frac{t - t_c}{h}\right)$$

Experimental setup:

Infrared Radiation:

Device support

AlO plate

IR beam

Cu plates

Bi_2Te_3 elements

Results:

Observing a sinusoidal instability in the power source.

Power

similar tc times

*tc is the critical time of both of the systems according to their respective functions where they are at a minimum

Voltage

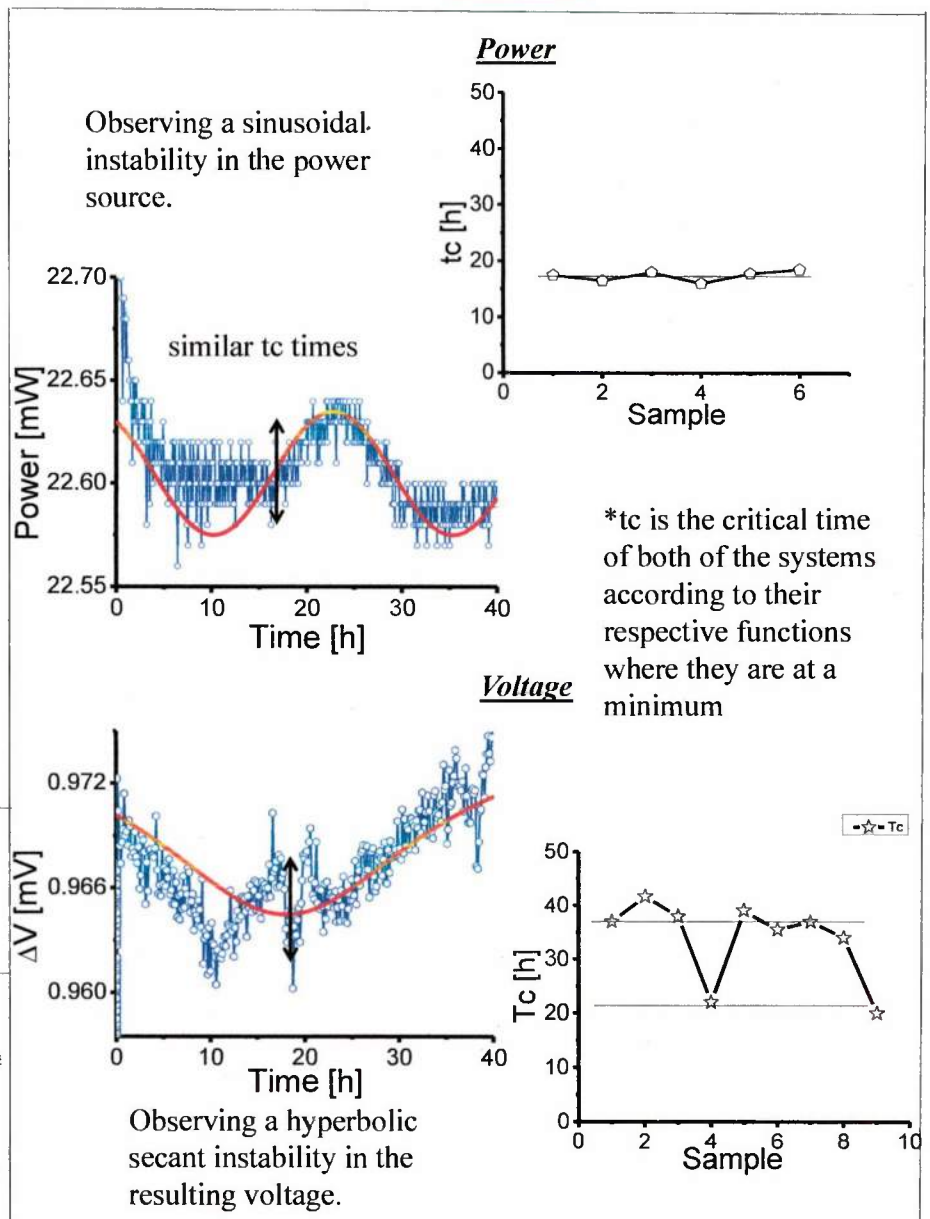Observing a hyperbolic secant instability in the resulting voltage.

Conclusion:

I. There is a correlation between the parameters between the two functions, specifically with tc.

The nano-power generator fabricated with thin atomic layer deposited

G. Scarel,[1] V.D. Wheeler,[2] H.S. Mann,[1] B.N. Lang,[1] Z.J. Marinelli,[1] and B.C. Utter[1]

[1]Department of Physics and Astronomy, James Madison University, Harrisonburg VA 22807
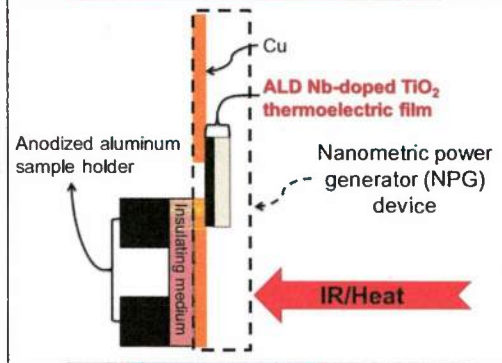
[2]U.S. Naval Research Laboratory, Washington D.C. 20375

Abstract:

Can infrared (IR) radiation [1,2] generate voltage on a nano-power generator (NPG) with active element consisting of an atomic-layer deposited (ALD) film [3,4]?

Experimental setup:

References:

[1] R. J. Parise and G. F. Jones, Collection of Technical papers–2nd International Energy Conversion Engineering Conference, 1172 (2004).
[2] Y. Schwab et al., Complexity 19, 44 (2013).
[3] J. Niemelä et al., Thin Solid Films 551, 19 (2014).
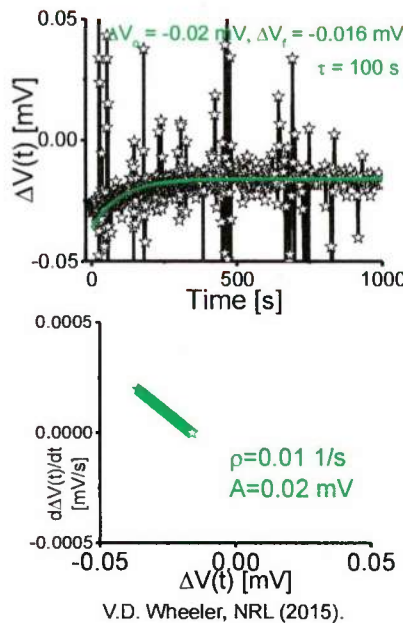[4] H.S. Mann et al., J. Vac. Sci. Technol. A 33, 01A124 (2015).

Result-1:

68.4 nm thick Nb-doped TiO_2 on borosilicate glass, resistivity = 1.4 10-5 Ω m (~ graphite)

$\Delta V_o = -0.0045$ mV
$\Delta V_f = 0.0023$ mV
$\tau = 100$ s

$\rho = 0.01$ 1/s
A = 0.0045 mV
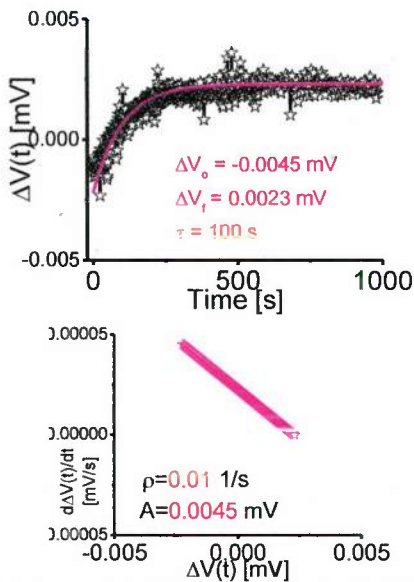
H.S. Mann et al., J. Vac. Sci. Technol. A 33, 01A124 (2015).

Result-2:

TiO_2:TiN ~2 nm:~2 nm on glass, sheet resistance = 26700 Ohms/sq

$\Delta V_o = -0.02$ mV, $\Delta V_f = -0.016$ mV
$\tau = 100$ s

$\rho = 0.01$ 1/s
A = 0.02 mV

V.D. Wheeler, NRL (2015).

Result-3:

TiO_2:TiN ~5 nm:~5 nm glass, sheet resistance = 634 Ohms/sq

$\Delta V_o = -0.009$ mV,
$\tau = 150$ s,
$\Delta V_f = 0.0075$ mV

-0.0066 1/s

A = 0.00899 mV
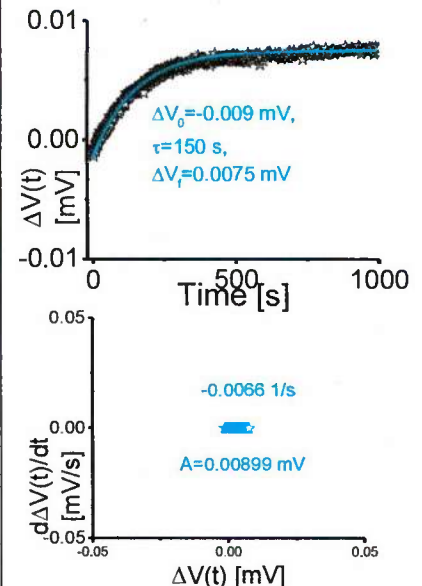
V.D. Wheeler, NRL (2015).

Acknowledgments

Outlook

These preliminary results suggest that power generation with ALD NPG might be significantly improved by engineering the film resistance.

Conclusions

I. The IR radiation is able to excite the voltage on a NPG.
II. Voltage and temperature difference have the same time constant.
III. Correct resistivity to achieve larger voltage rise upon starting the illumination with IR radiation still needs to be found.

Giovanna Scarel

Department of Physics and Astronomy
James Madison University,
Harrisonburg (VA), U.S.A.

"*Atomic layer deposition for rare earth oxides and thermoelectric thin films*".

Atomic layer Deposition: Russia 2015

Moscow (Russian Federation),
September 21-23 2015

OUTLINE

• ALD of Lu_2O_3 films
• ALD of GeO_2 films } Part A

Part B

• ALD films for **infrared power generation**

INTRODUCTION

- Unexplored avenues in ALD

- Enhance partnership between ALD communities in Russia and Worldwide

- Innovative applications and fundamental research enabled by ALD

ALD of Lu_2O_3 films

General properties of rare earth oxides:

La^{3+}	Ce^{3+}	Pr^{3+}	Nd^{3+}	Sm^{3+}	Eu^{3+}	Gd^{3+}	Tb^{3+}	Dy^{3+}	Ho^{3+}	Er^{3+}	Tm^{3+}	Yb^{3+}	Lu^{3+}
0.123	0.115	0.114	0.112	0.106	0.106	0.104	0.100	0.099	0.098	0.096	0.094	0.093	0.092

Rare earth element ionic radii in nm: Y. Sakabe et al., Jpn. J. Appl. Phys. **41**, 5668 (2002)

Higher ionic radius

$\Rightarrow$ Lower sensitivity to **moisture**

$\Rightarrow$ Lower chemical activity with **Si**

ALD of Lu$_2$O$_3$ films

$\{[C_5H_4(SiMe_3)]_2LuCl\}_2$ at 195 °C
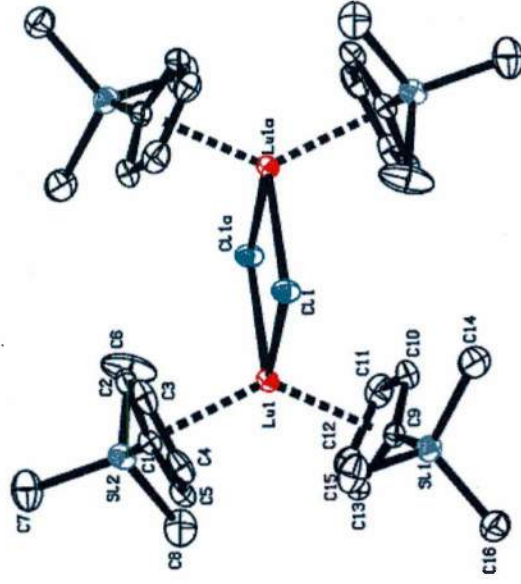
H. Schumann, I.L. Fedushkin, M. Hummert, G. Scarel, E. Bonera, and M. Fanciulli,
"*Crystal and molecular structure of $[(\eta^5\text{-}C_5H_4SiMe_3)_2LuCl]_2$ – a precursor for the production of Lu_2O_3 films*".
Z. Naturforsch. **59b**, 1035 (2004)
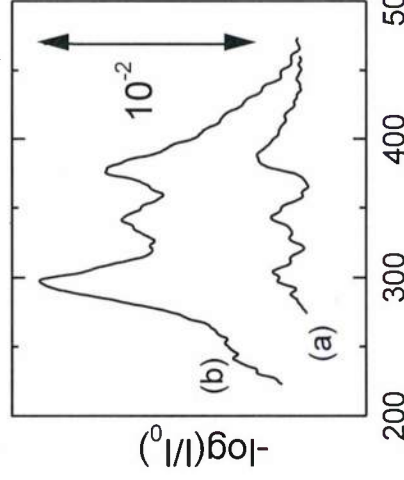
G. Scarel, E. Bonera, C. Wiemer, G. Tallarida, S. Spiga, M. Fanciulli, I.L. Fedushkin, H. Schumann, Y. Lebedinskii, and A. Zenkevich, "*Atomic-layer deposition of Lu_2O_3*". Appl. Phys. Lett. **85**, 630 (2004)

$\kappa \cong 12\pm1$

Cubic Lu$_2$O$_3$ film after annealing

ALD of Lu_2O_3 films

... otherwise Lu is used for ternary compounds!

1) L. Nyns et al., JVST A **30**, 01A120 (2012); Lu-aluminates using $(Lu(iPrCp)_3)$ tris(isopropyl cyclopentadienyl) Lu; $\kappa \cong$ **12.7** with large Lu content

2) H. Wang et al., ESSL **12**, G13 (2009); lanthanum-Lu ternaries using Lu tris(N,N'-diethyl-formamidinate); $\kappa \cong$ **28±1 for LaLuO$_3$**

3) M. Roeckerath et al., TSF **517**, 210 (2008); lanthanum-Lu ternaries using Lu(thd)3, Lu (2,2,6,6-tetramethyl-3,5-heptadionato)$_3$); $\kappa \cong$ **17 for LaLuO$_3$**

controversy

Consiglio Nazionale delle Ricerche
Istituto per la Microelettronica e Microsistemi - Sezione di Agrate Brianza

Laboratorio MDM

JAMES MADISON UNIVERSITY

PHYSICS AND ASTRONOMY
JAMES MADISON UNIVERSITY

ALD of Lu₂O₃ films

Unique and precise study of the band alignment of Lu₂O₃ on Si(100) and on Ge(100)

Similar results
for **Lu₂O₃** on **Ge(100)**

conduction band offset (CBO)

valence band offset (VBO)

G. Seguini *et al.*, Appl. Phys. Lett. **85**, 5316 (2004)

ALD of Lu_2O_3 films

Crystalline structure from infrared spectroscopy

Lu₃O₃

296

289
275
270

Lu_3O_3
235

Yb
Gd Tb

Absorbance (arb. un.)

200   400

Frequency (cm^{-1})
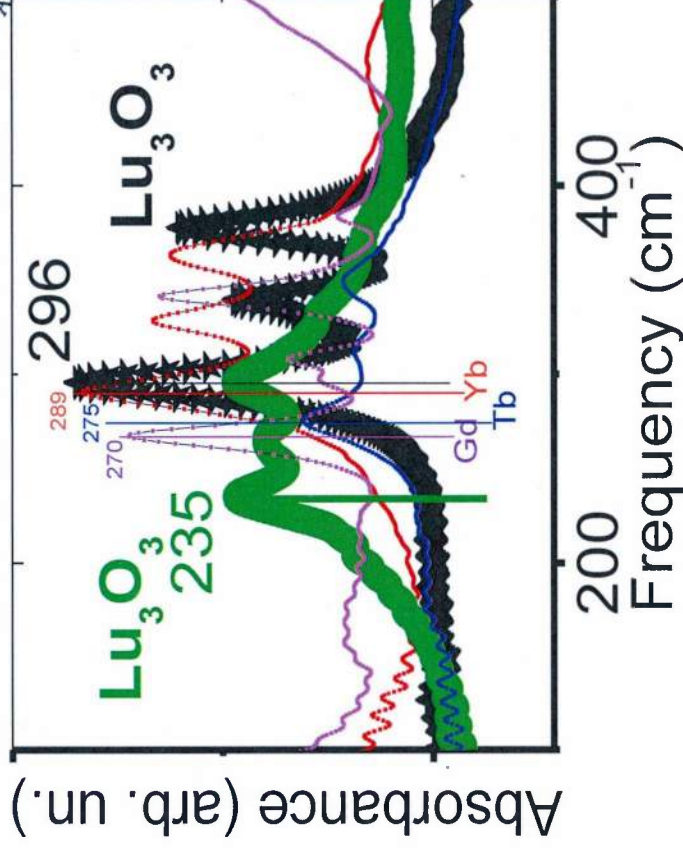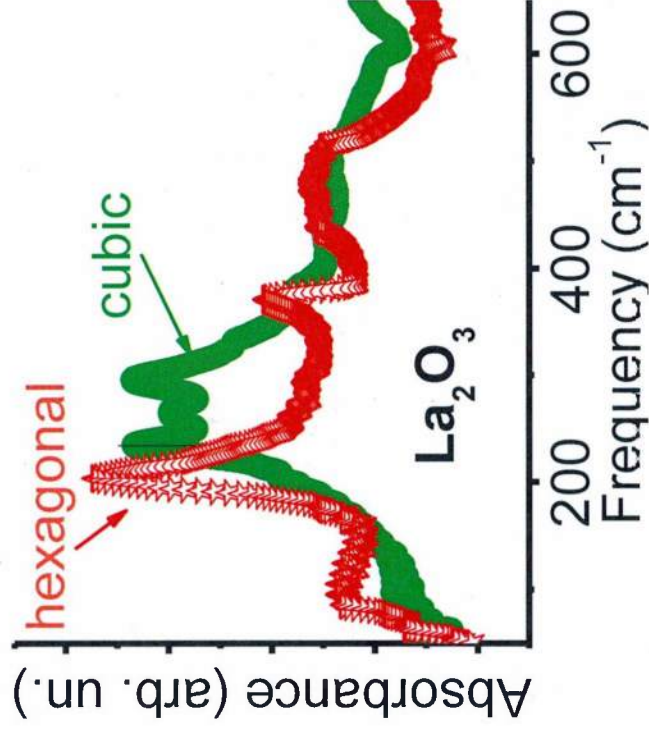
Cubic structure of some rare **earth oxides after annealing**

cubic

hexagonal

La_2O_3

Absorbance (arb. un.)

200   400   600

Frequency (cm^{-1})

ALD of GeO$_2$ films

SiO$_2$ and GeO$_2$ films are difficult to create with ALD
because thermal oxidation of
silicon and germanium precursors
is not very efficient
and results in the formation of
various sub-oxide species

ALD of GeO$_2$ films

... Ge precursors mostly used for chalcogenide compounds!

1) S.B. Kim et al., Chem. Mater. **26**, 3065 (2014); GeS using Ge(II) cyclic amides from N^2,N^3-di-tert-butylbutane-2,3-diamine

2) K. Knapas et al., Chem. Mater. **22**, 1386 (2010); GeTe using (1,4-dioxane complex of GeCl$_2$) i.e. GeCl$_2$·C$_4$H$_8$O$_2$. Also here Ge(II).

3) B.J. Choi et al., Chem. Mater. **21**, 2386 (2009), GST films using tetraisobutyl germanium, Ge(i-C$_4$H$_9$)$_4$. Here Ge(IV)

JAMES MADISON UNIVERSITY

JAMES MADISON UNIVERSITY PHYSICS AND ASTRONOMY

Consiglio Nazionale delle Ricerche
Istituto per la Microelettronica e Microsistemi - Sezione di Agrate Brianza
Laboratorio MDM

ALD of GeO$_2$ films

New precursor design:

(dpp-BIAN)Ge   dpp-BIAN = 1,2-bis[(2,6-diisopropylphenyl)imino]acenaphthene)

- compound based on Ge(II)
- monomeric two-coordinate Ge derivative
- volatile
- solid
- easy to handle at room temperature

C H N Ge

Ar =

iPr   iPr

Ge—N–Ar

Ar–N
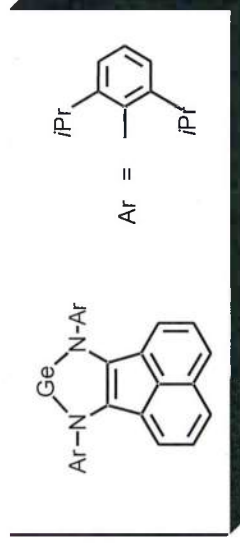
I.L. Fedushkin et al., Organometallics **23**, 3714 (2004)

JAMES MADISON UNIVERSITY

JAMES MADISON UNIVERSITY PHYSICS AND ASTRONOMY

Consiglio Nazionale delle Ricerche
Istituto per la Microelettronica e Microsistemi - Sezione di Agrate Brianza

Laboratorio MDM

ALD of GeO$_2$ films

Role of O$_3$ in changing the oxidation state of Ge(II) to Ge(IV):
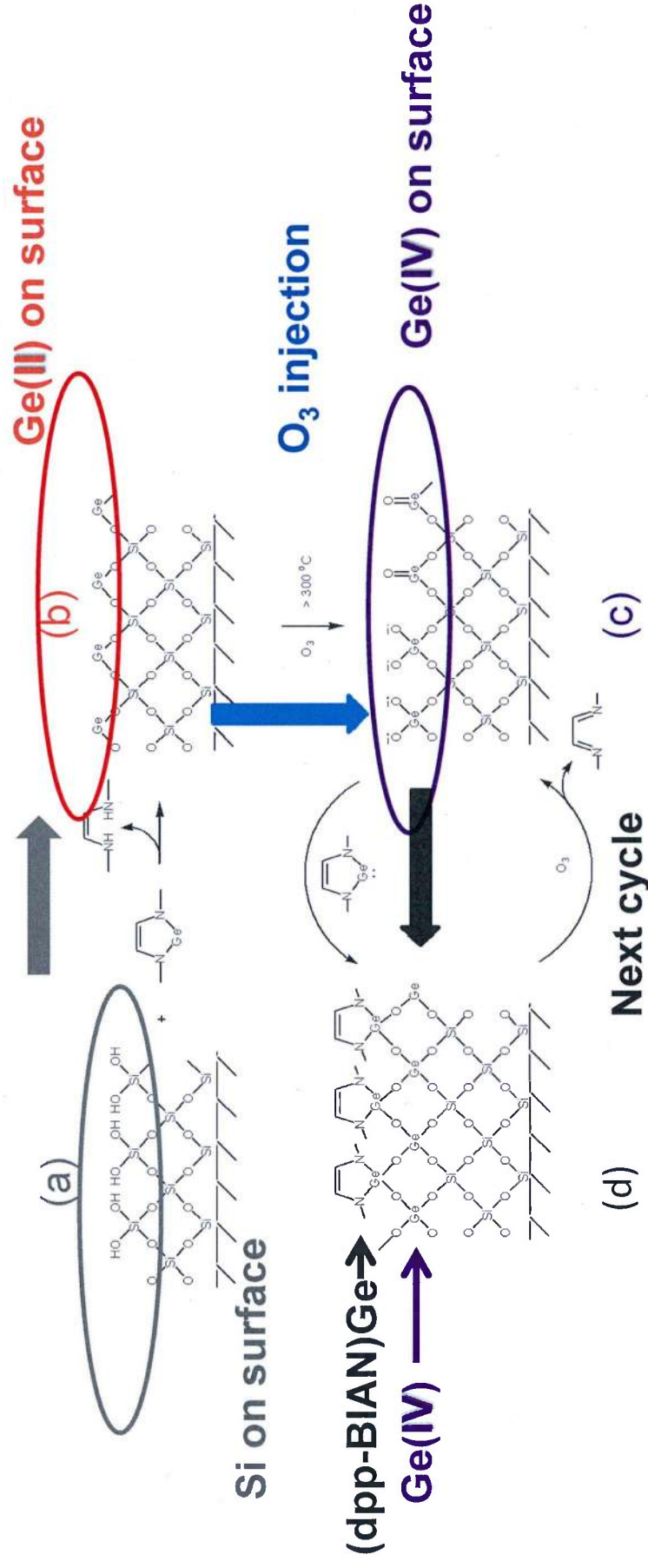
Ge(II) on surface

Ge(IV) on surface

O$_3$ injection

Si on surface

(dpp-BIAN)Ge → Ge(IV)

Next cycle

(a) (b) (c) (d)

> 300 °C

M. Perego, G. Scarel, M. Fanciulli, I.L. Fedushkin, and A.A. Skatova, *"Fabrication of GeO$_2$ layers using a divalent Ge precursor"*. Appl. Phys. Lett. **90**, 162115 (2007)

ALD of GeO₂ films

Film composition:

(dpp-BIAN)Ge and O₃: T_{growth} = 300 °C,

$T_{sublim.}$ = 225 °C

Pure **GeO₂** on Si(100)

No Ge sub-oxides!

GeO₂ on chemically oxidized Si(100)

GeO₂ on H-terminated Si(100)

High resolution XPS

- ○ Experimental data
- – – – Background
- —— Fitting result

Ge 3d   33.049 eV

33.156 eV

C 1s 284.5 eV
Charge reference

(a)

(b)

Intensity (arb. units)

Binding Energy (eV)

M. Perego, G. Scarel, M. Fanciulli, I.L. Fedushkin, and A.A. Skatova,
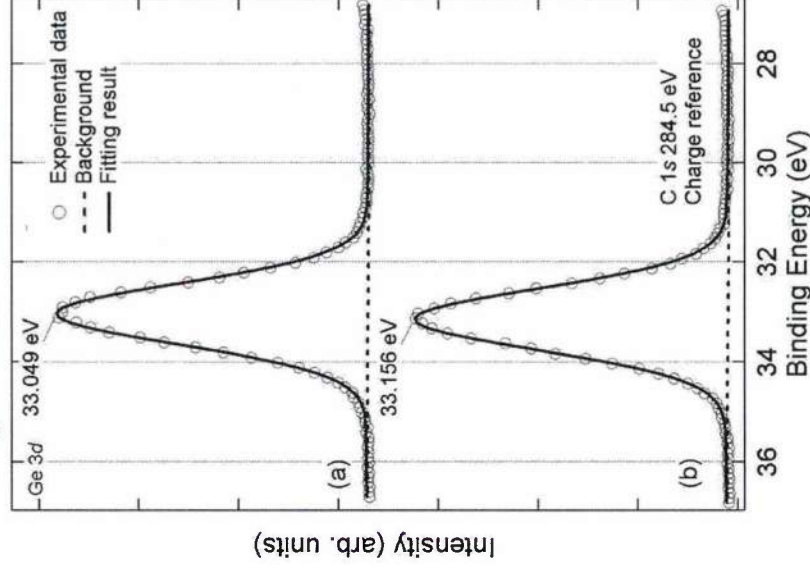*"Fabrication of GeO₂ layers using a divalent Ge precursor"*.
Appl. Phys. Lett. **90**, 162115 (2007)

JAMES MADISON UNIVERSITY
PHYSICS AND ASTRONOMY

JAMES MADISON UNIVERSITY.

Consiglio Nazionale delle Ricerche
Istituto per la Microelettronica e Microsistemi – Sezione di Agrate Brianza
Laboratorio MDM

ALD of GeO$_2$ films

Film electric properties:

XPS: energy loss features

O 1s

(dpp-BIAN)Ge and O$_3$: T_{growth} = 300 °C,
$T_{sublim.}$ = 225 °C

GeO$_2$ band gap = 5.8 eV
CBO on GeO$_2$/Ge: 0.6 eV
VBO on GeO$_2$/Ge: 4.5 eV
κ ~ 5.5

M. Perego, G. Scarel, M. Fanciulli, I.L. Fedushkin, and A.A. Skatova, "*Fabrication of GeO$_2$ layers using a divalent Ge precursor*". Appl. Phys. Lett. **90**, 162115 (2007)
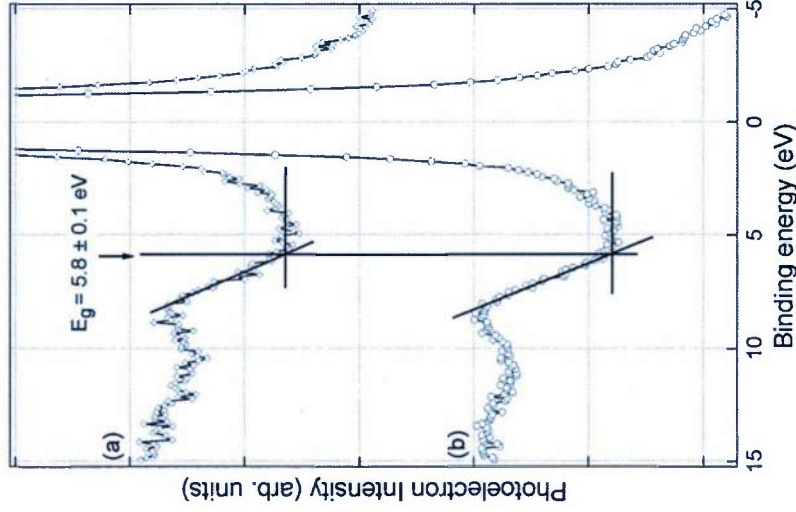
JAMES MADISON UNIVERSITY

PHYSICS AND ASTRONOMY — JAMES MADISON UNIVERSITY

Consiglio Nazionale delle Ricerche
Istituto per la Microelettronica e Microsistemi – Sezione di Agrate Brianza
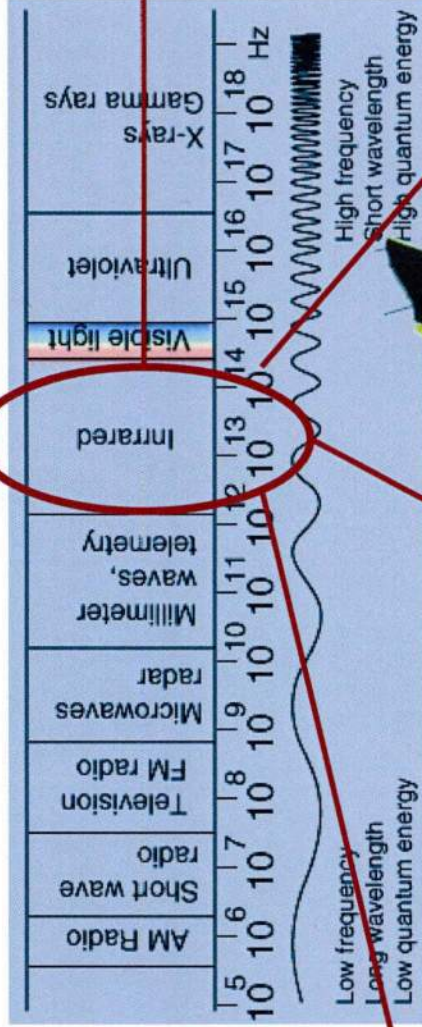Laboratorio MDM

Summary
Part A

- **Novel precursors** can be discovered

- **Pure** oxides and compounds can be prepared

- Detailed and precise characterization of the **electric properties of interfaces** can be enabled

ALD films for infrared
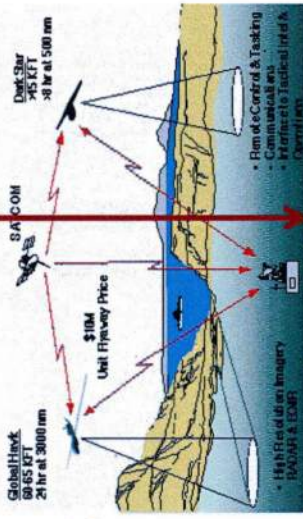# power generation

satellites

backpacks

ships

cars

ALD films for **infrared power generation**

Experimental set-up with macro-device:
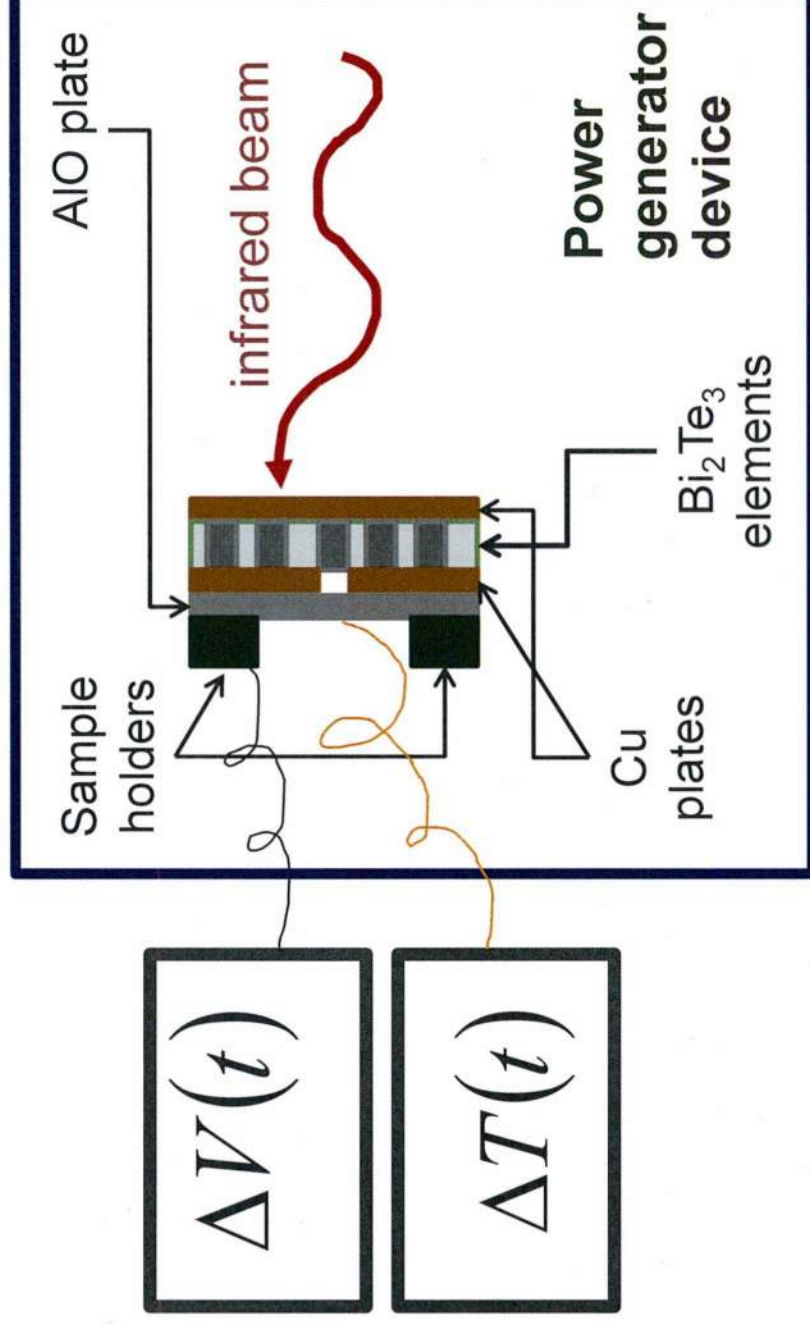
ALD films for infrared power generation

Effects of radiation on the device:

infrared radiation
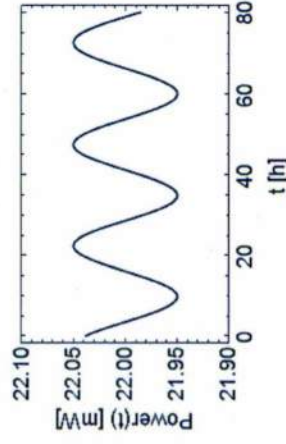
Hits the device at variable power

Perturbs the charge density on the device
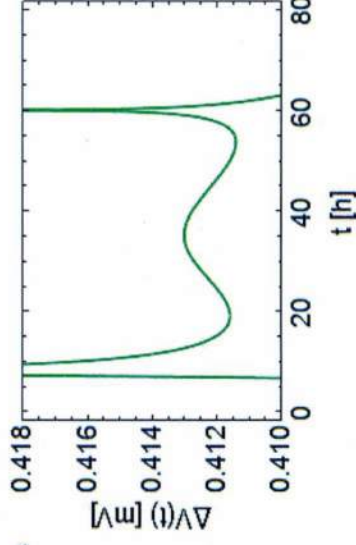
Generates a variable non-periodic voltage difference $\Delta V(t)$

At the 30th hour after starting the illumination

ALD films for infrared power generation

Remarkable similarity between the experimental data ......
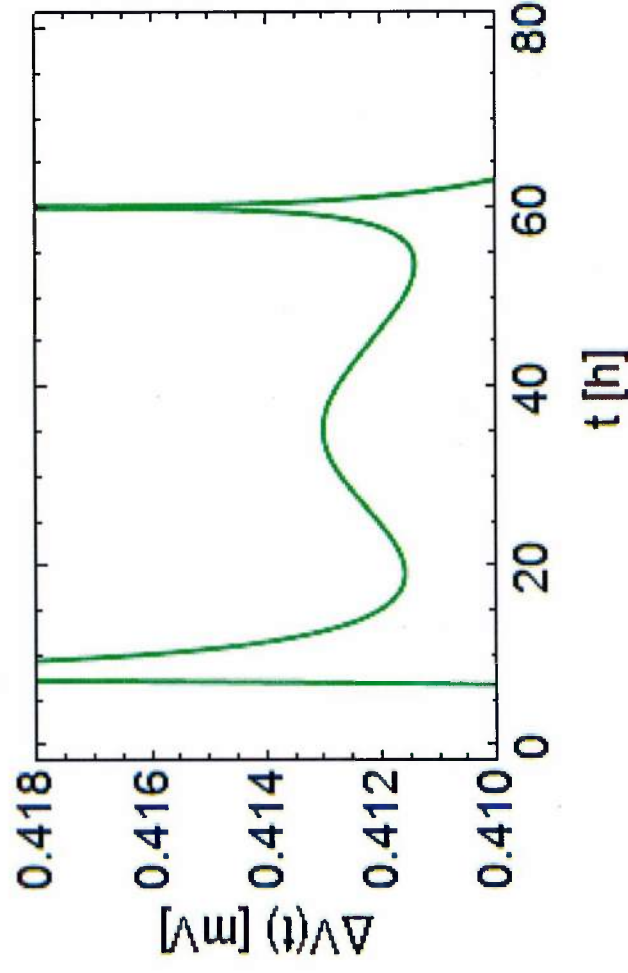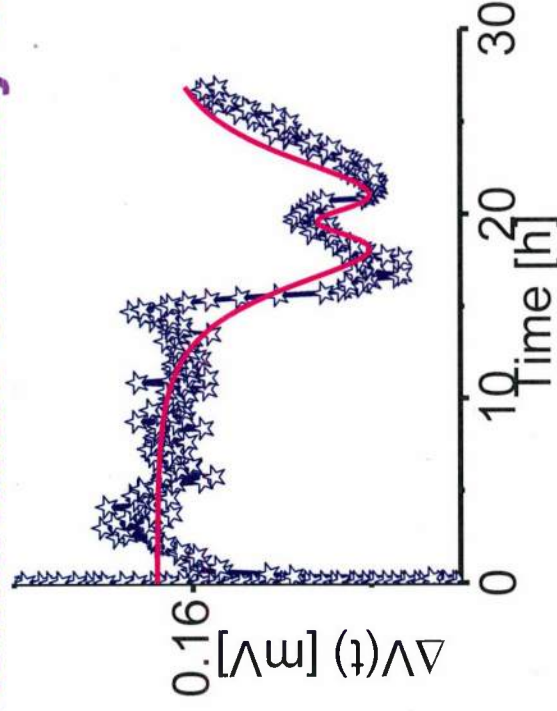
... and our model:

$\Rightarrow$ infrared radiation generates an USABLE electric signal on the power generator device

JAMES MADISON UNIVERSITY PHYSICS AND ASTRONOMY

JAMES MADISON UNIVERSITY

DEPARTMENT OF THE NAVY — ONR — Science & Technology

MADISON TRUST
FOSTERING INNOVATION AND STRATEGIC PHILANTHROPY

ALD films for infrared power generation

Core of the JMU discovery:

The **surface charge** on the power generator device *breaks the periodicity* in the relationship between the **time dependence** of the **radiation power** **below a critical threshold** and the **time dependence** of the **voltage** produced by the device.

ALD films for infrared power generation

Thin ALD films enable:

- **nano**-power generators
- tuning active layer **resistivity**
- large **area** coverage

ALD films for infrared power generation

Experimental set-up with nano-power generator:

H.S. Mann, B.N. Lang, Y. Schwab, J.-P. Niemelä,
M. Karppinen, and G. Scarel,
*"Infrared and thermoelectric power generation
in thin atomic layer deposited Nb-doped TiO$_2$ films"*.
J. Vac. Sci. Technol. A **33**, 01A124 (2015)

ALD films for infrared power generation

Results with nano-power generator:

68.4 nm thick Nb-doped TiO_2 on borosilicate glass,
resistivity = **1.4 10^{-5} Ω m** ($\sim$ graphite)

ΔV_o = -0.0045 mV
ΔV_f = 0.0023 mV
τ = 100 s

ρ=0.01 1/s
A=0.0045 mV
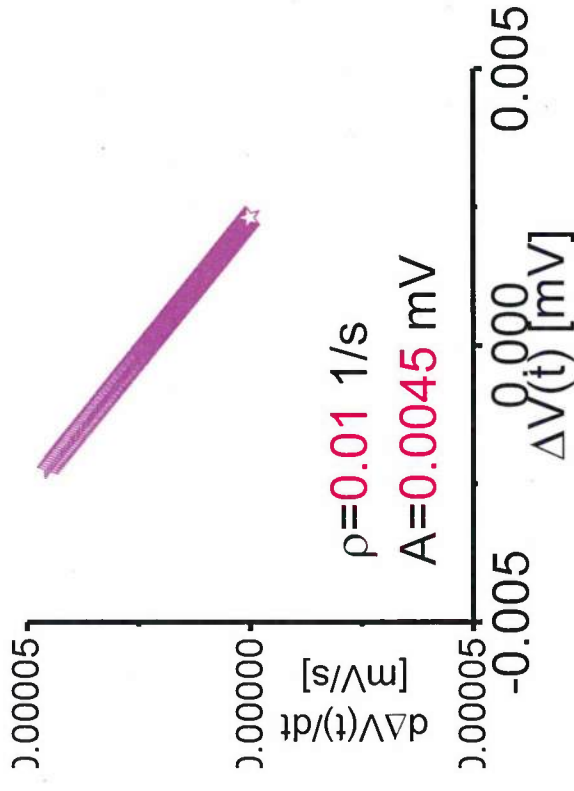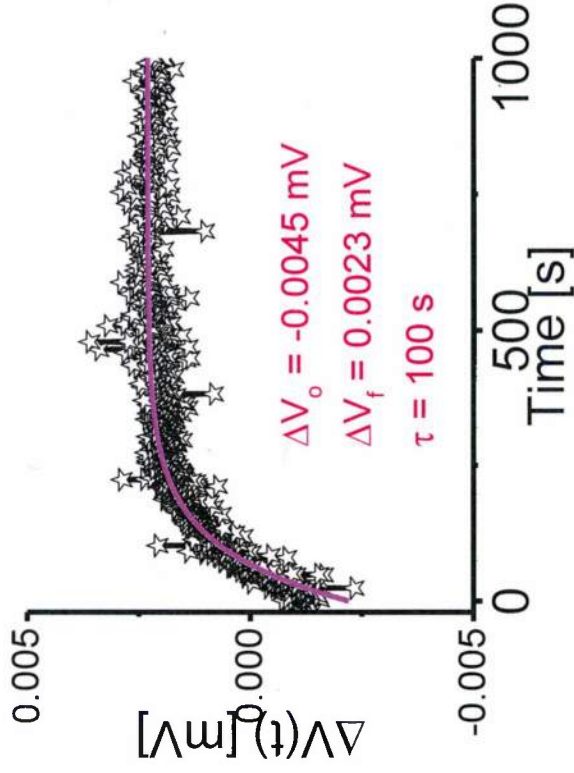
H.S. Mann, B.N. Lang, Y. Schwab, J.-P. Niemelä,
M. Karppinen, and G. Scarel,
"Infrared and thermoelectric power generation
in thin atomic layer deposited Nb-doped TiO_2 films".
J. Vac. Sci. Technol. A **33**, 01A124 (2015)

ALD films for infrared power generation:

Results with nano-power generator:

Nanolaminate TiO_2/TiN 2 nm/2 nm on glass,

Sheet resistance = **26700 Ω/sq**

$\Delta V_0 = -0.02$ mV, $\Delta V_f = -0.016$ mV

$\tau = 100$ s

$\rho = 0.01$ 1/s
$A = 0.02$ mV

$\Delta V(t)$ [mV]

Time [s]

$d\Delta V(t)/dt$ [mV/s]

$\Delta V(t)$ [mV]
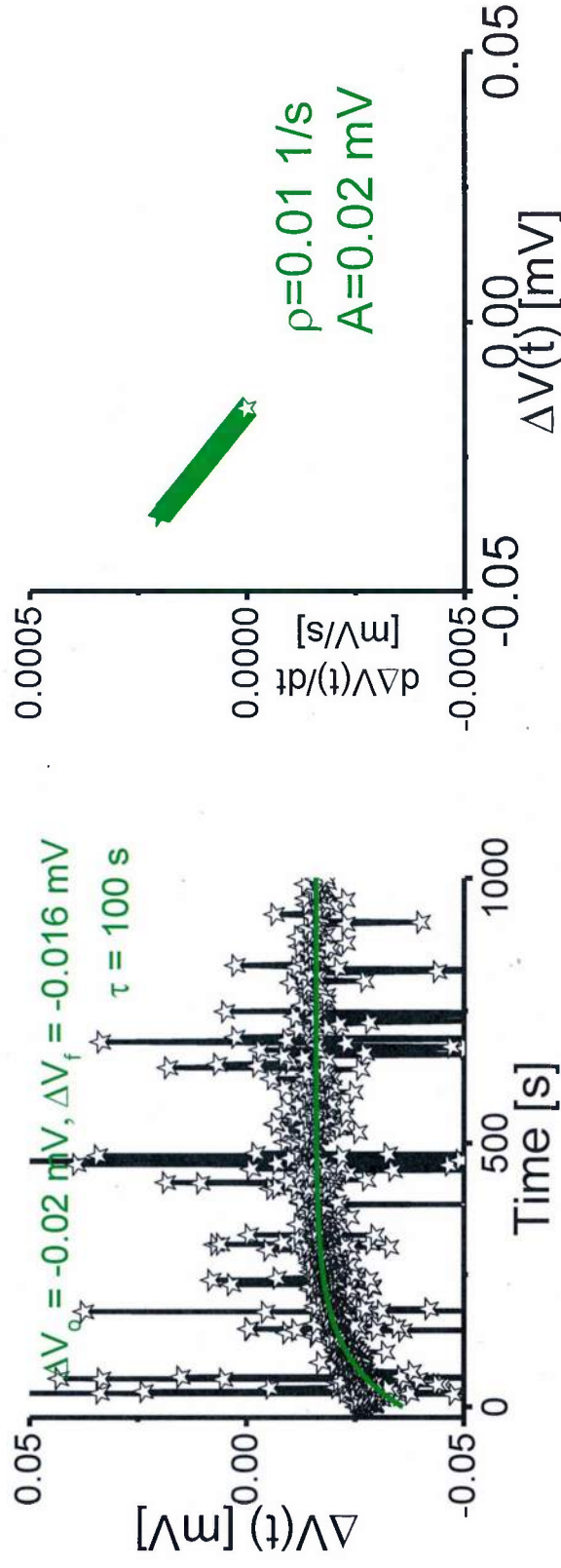
Dr. Virginia Wheeler
Naval Research Laboratory
Washington D.C. (U.S.A.)

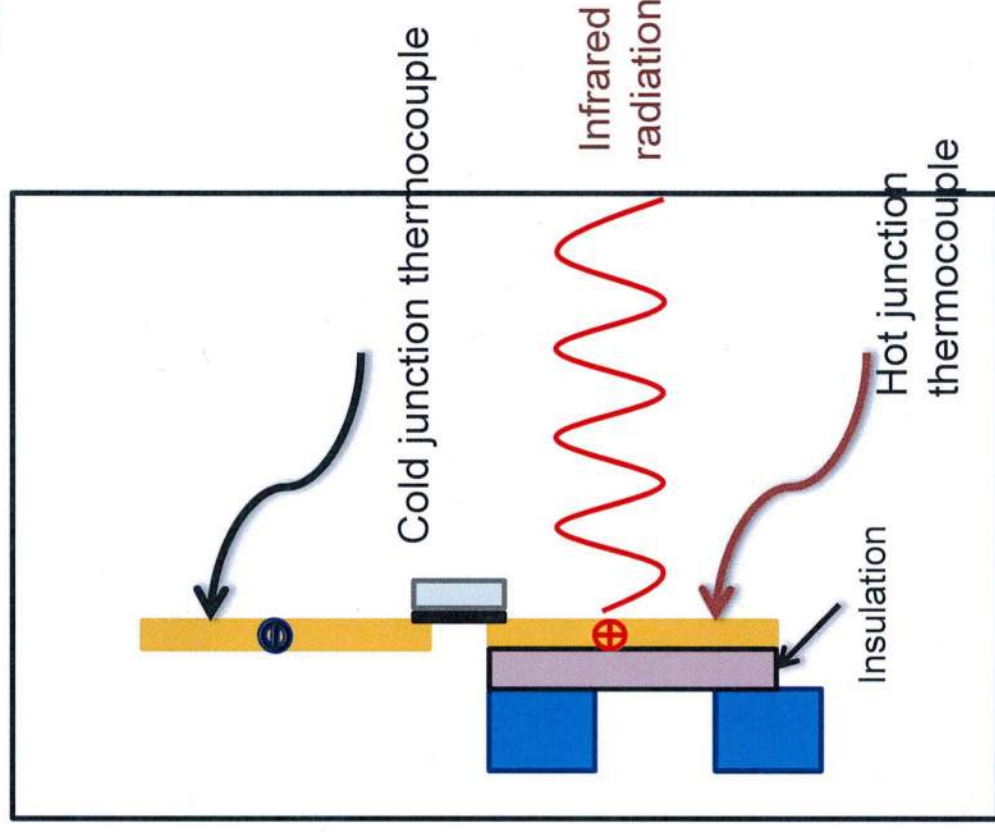JAMES MADISON UNIVERSITY PHYSICS AND ASTRONOMY

JAMES MADISON UNIVERSITY

MADISON TRUST
FOSTERING INNOVATION AND STRATEGIC PHILANTHROPY

ALD films for infrared power generation

Results with nano-power generator:

68.4 nm thick Nb-doped TiO_2 on borosilicate glass, resistivity = **1.4 10^{-5} Ω m** (~ graphite)

Less noise, small jump in $\Delta V(t)$

Nanolaminate TiO_2/TiN 2 nm/2 nm on glass, Sheet resistance = **26700 Ω/sq**

More noise, larger jump in $\Delta V(t)$

Summary Part B

ALD can contribute in many ways to improve efficiency of the active layer in **nano-power generators** for **infrared power generation** through:

- **Film thickness?**

- **Film resistivity?**

- **Film structure and architecture?**

Acknowledgements

- **Marco Fanciulli**, CNR-INFM MDM National Laboratory Agrate Brianza (MI), Italy

- **Andrei Zenkevich**, Moscow Institute of Physics and Technology, Moscow (Russian Federation)

- **I. L. Fedushkin**, G. A. Razuvaev Institute of Organometallic Chemistry, Russian Academy of Sciences, Nizhny Novgorod, Russia

- **Brian C. Utter**, Department of Physics and Astronomy, JMU, U.S.A.

- **Virginia D. Wheeler** and **Marc Currie**, Naval Research Laboratory, Washington D.C., U.S.A.

Funding

- PAIS-INFM 2003-2004 **REOHK**: *"Rare earth oxides as high-κ dielectrics for CMOS"*.

- **Joint Russia-Italy Project 2005** (funded by Russian Government): *"Innovative high-κ films for CMOS devices"*

- **Joint Italy-Russia Project 2003-2004** (funded by the Italian Ministry for Foreign Affairs): *"Innovative high-κ films for CMOS devices"*

- **U.S. Office of Naval Research** (awards # N000141410378 and N000141512158), 2014-2017: *"The exploitation of the electric contributions in infrared power generation"*

- The Madison Trust—Fostering Innovation and Strategic Philanthropy - Innovation Grant, 2014: *"From JMU to the World: embracing the need of new energy sources"*

- The JMU Center for Materials Science and Department of Physics and Astronomy

Students at JMU

Students – JMU:

Yosyp Schwab

Harkirat S Mann

Brian N. Lang

Graham P. Gearhart

Tara R. Jobin

Justin M. Kaczmar

Zach J. Marinelli

Aidan L. Gordon

Kyle A. Britton

Scientific
Research
Publishing

Decoupling the Electrical and Entropic Contributions to Energy Transfer from Infrared Radiation to a Power Generator

Aidan L. Gordon, Yosyp Schwab, Brian N. Lang, Graham P. Gearhart, Tara R. Jobin, Justin M. Kaczmar, Zachary J. Marinelli, Harkirat S. Mann, Brian C. Utter*, Giovanna Scarel*

Department of Physics and Astronomy, James Madison University, Harrisonburg, USA
Email: *utterbc@jmu.edu, *scarelgx@jmu.edu

Abstract

The interaction between infrared radiation and a power generator device in time is studied as a route to harvest infrared, and possibly other electromagnetic radiations. Broadening the spectrum of the usable electromagnetic spectrum would greatly contribute to the renewable and sustainable energy sources available to humankind. In particular, low frequency and low power radiation is important for applications on ships, satellites, cars, personal backpacks, and, more generally, where non-dangerous energy is needed at all hours of the day, independent of weather conditions. In this work, we identify an electric and an entropic contribution to the energy transfer from low power infrared radiation to the power generator device, representing electrical and thermal contributions to the power generation. The electric contribution prevails, and is important because it offers multiple ways to increase the voltage produced. For example, placing black-colored gaffer tape on the illuminated face doubles the voltage produced, while the temperature difference, thus the entropic contribution, is not sensitive to the presence of the tape. We recognize the electric contribution through the fast changes it imparts to the voltage output of the power generator device, which mirror the instabilities in time of the infrared radiation. The device thus acts as sensor of the infrared radiation's behavior in time. On the other hand, we distinguish the entropic contribution through the slow changes it causes to the voltage output of the power generator device, which reflect the relative delay with which the two faces of the device respond to thermal perturbations.

Keywords

Infrared, Power Generators, Energy Harvesting, Electric Contribution

---

*Corresponding authors.

1. Introduction

A power generator (PG) device can be used to harvest electromagnetic (EM) and, in particular, infrared (IR) radiation. The interaction between the radiation and the device is a complex phenomenon of energy transfer (ΔE). The rate of energy transferred from the EM radiation per area a of the device is the Poynting vector $|S| = |E \times H| = P/a$, where E and H are the electric and magnetic fields, respectively, and P is power. Therefore, because of E and H, the interaction between radiation and device involves the charges on the device surface. Electromagnetic radiation with large frequency ν interacts through, e.g., Compton scattering [1], X-ray photoelectron effect [2], photoelectric effect [3], photovoltaic effect [4], and plasmon generation [5]. Electromagnetic radiation with low frequency ν, e.g. in the IR and microwave regions, resonates with molecular rotation and oscillation frequencies [6] or generates polaritons [7]-[10]. When the photon frequency ν or energy $h\nu$, where h is Planck's constant, do not match with the frequency or the energy of a specific phenomenon involving charges, the energy of the EM radiation contributes to temperature T changes. In photosynthesis this phenomenon is known as internal conversion [11].

We name the energy transferred from the EM radiation to a PG device through the action of the electric E and magnetic H fields as the electric contribution:

$$\Delta E_{el} = q\Delta V, \tag{1}$$

where q is the charge and V voltage. We name the energy transferred through changes in temperature T at entropy Σ as the entropic contribution:

$$\Delta E_{en} = \Sigma\Delta T. \tag{2}$$

The energy transferred from IR and microwave radiation is usually associated with the entropic contribution in Equation (2). For example, sun light gives the sensation of temperature increase, and therefore of warmth, on human skin. The microwave radiation in microwave ovens is used to increase the temperature, *i.e.*, cook food and heat-up beverages. Similarly, through laser radiation it is possible to increase temperature, even with nanoscale control [12].

The effects of the electric contribution $\Delta E_{el} = q\Delta V$ are less apparent in the energy transfer from low frequency and low power EM radiation. In the current literature, the existence of the electric contribution is acknowledged [13]-[16], but the interplay between the electric and the entropic contributions is not investigated. Specifically, there is a lack of knowledge of 1) the possibility of decoupling the electric from the entropic contributions, 2) the factors that promote the electric over the entropic contribution, or *vice-versa*, 3) the existence of a threshold where one contribution prevails over the other, and 4) the benefits of the electric over the entropic contributions, or *vice-versa*.

In this work we aim at decoupling ΔE_{el} and ΔE_{en} in a PG device illuminated by low power IR radiation. The device is expected to respond to the entropic contribution by exploiting the Seebeck effect [17]-[20], *i.e.* producing a voltage difference ΔV directly proportional to the temperature difference ΔT applied to the two faces of the PG device, so that $\Delta V = -S\Delta T$. Here, S is the Seebeck coefficient. On the other hand, we expect the PG device to also respond to the electric contribution through its capacitor-type of structure consisting of a sequence of conducting and insulating layers, as illustrated in **Figure 1**. For the device used in this work, the sequence is, starting from the face illuminated by the IR radiation, a copper (Cu) plate, a layer of pillars made of adoped Bi_2Te_3-based alloy, another Cu plate, and, finally, an alumina (AlO) plate. On the Cu plates there are electrons whose surface density $\sigma = q/a$ is sensitive to the E and H fields of the IR radiation, thus enabling changes in the electric contribution $\Delta E_{el} = q\Delta V$.

In our experiment, the voltage difference $\Delta V(t)$, generated by the PG device through the electric and the entropic contributions, and the temperature difference $\Delta T(t)$, related to the entropic contribution, are observed as a function of time t. The measurements capture the first minutes after starting the illumination, and in the 30 hours thereafter. We hypothesize that changes in $|S(t)| \times a = |E(t) \times H(t)| \times a = P(t)$ slowly vary the amplitude of the surface electron density $\sigma(r,t)$. To prove this hypothesis, we study the power $P(t)$ of the IR radiation using a power-meter sensor and compare its behavior with that of $\Delta V(t)$ and $\Delta T(t)$.

Summarizing, we consider the total energy transfer in time from the IR radiation to a PG device as the sum of the electric and the entropic contributions such that:

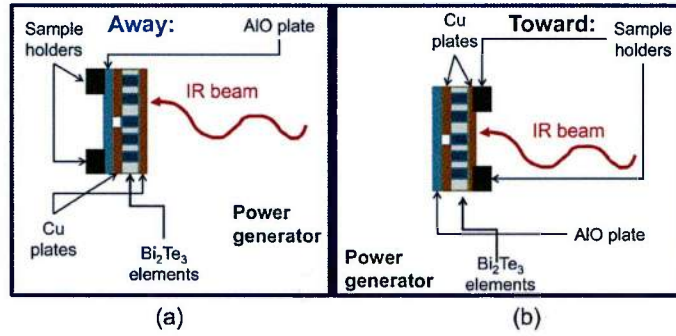$$\Delta E(t)_{tot} = q(t)\Delta V(t) + \Sigma\Delta T(t). \tag{3}$$

Figure 1. Schematics of the *away* (a) and *toward* (b) architectures of the PG device. In the *away* architecture (a) the face of the PG device exposed to the IR radiation is free from contact with the sample holder. In the *toward* architecture (b), the illuminated face is in contact with the sample holder. The PG device is a stack of conducting (Cu plates), non-conducting (AlO plate), and semiconducting (set of pillars made of a doped Bi_2Te_3-based alloy) layers.

Consequently, we assume the voltage difference $\Delta V(t)$ produced by the PG device in time to be the addition of two summands:

$$\Delta V(t) = \frac{\Delta E(t)_{tot}}{q(t)} + \left(-\frac{\Sigma \Delta T(t)}{q(t)} \right). \tag{4}$$

The first summand relates to the electric and the second to the entropic contribution. The term $S = -\Sigma/q(t)$ can be associated with the Seebeck coefficient.

We will show that with the low power irradiation employed in our measurements, the electric contribution can be decoupled from the entropic contribution, and largely dominates. Decoupling the two contributions is important for IR energy harvesting, because the electric contribution offers a variety of ways to increase the voltage produced by the PG device, e.g. by placing black-colored gaffer tape on the illuminated face of the device, as we will show in Appendix-1. The entropic contribution, instead, is limited by the temperature difference $\Delta T(t)$ established between the two faces of the PG device.

2. Experimental Set-Up

For this experiment, continuous broadband IR radiation in the middle IR (MIR) region (*i.e.* frequency between $350 - 7500 \, cm^{-1}$, or wavelength between $20 - 2.2 \, \mu m$) was produced by a globar (Q301) source. The power $P(t)$ of the IR radiation was monitored versus time using a power-meter sensor Coherent Power Max RS PS19, sensitive to the $300 - 11000 \, nm$ wavelength range, and to the $100 \, \mu W$ to $1 \, W$ power range.

The voltage difference $\Delta V(t)$, generated by the electric and the entropic contributions to ΔE_{tot} according to Equation (4), was produced using a PG device 07111-9L31-04B by Custom Thermoelectric Inc. The device consists of a sequence of layers: 1) a Cu plate on the face exposed to the IR radiation, 2) a layer of pillars made of a doped Bi_2Te_3-based alloy, 3) another Cu plate, and 4) an AlO plate. The Cu plate not illuminated by the IR radiation is non-continuous, as highlighted through the white hole in the left side of **Figure 1(a)** and **Figure 1(b)**. In the *away* architecture, illustrated in **Figure 1(a)**, we established the continuity by placing the sample holders, made of anodized aluminum, in contact with the non-continuous Cu plate. Thus, the Cu plate together with the sample holder behaves as the electrode of a capacitor. The illuminated Cu plate, instead, was free of contact with the sample holder. In the *toward* architecture, pictured in **Figure 1(b)**, we left non-continuous the Cu plate opposite to the IR radiation, while the illuminated Cu plate was kept in contact with the sample holder.

The temperatures $T_{iR}(t)$ and $T_{no-IR}(t)$ of the illuminated and non-illuminated faces, respectively, of the PG device were measured using OMEGA type E Ni-Cr/Cu-Ni thermocouple probes. The temperature difference $\Delta T(t)$ was obtained as $\Delta T(t) = T_{IR}(t) - T_{no-IR}(t)$. The trends of $\Delta V(t)$, $T_{IR}(t)$ and $T_{no-IR}(t)$ were measured using Keithley 2000 multi-meters. The data were collected using LabView 2012 and a National Instruments PXI-1042q communications chassis.

During the measurements, the PG device and the power-meter sensor were positioned vertically and at an angle of incidence $\theta_0 = 45°$ with respect to the IR radiation. The instrumentation was placed in a closed sample

compartment purged with N_2 to prevent disturbances for the whole duration of the measurements versus time of $P(t)$, $\Delta V(t)$, $T_{IR}(t)$ and $T_{no-IR}(t)$ [21]. The experimental parameters are summarized in **Table 1**.

3. Results and Discussion

a) Behavior in time of $P(t)$

In the 100 seconds immediately after starting the illumination of the power-meter sensor, $P(t)$, displayed in **Figure 2(a)**, rises exponentially as follows:

Table 1. Summary of the experimental parameters in the main text and in the appendices.

Main text		
IR frequency (μm)	Infrared angle of incidence (°)	PG device final layer
20 - 2.2	45	Cu
Appendices		
IR frequency (μm)	Infrared angle of incidence (°)	PG device final layer
20 - 2.2	30	Alumina
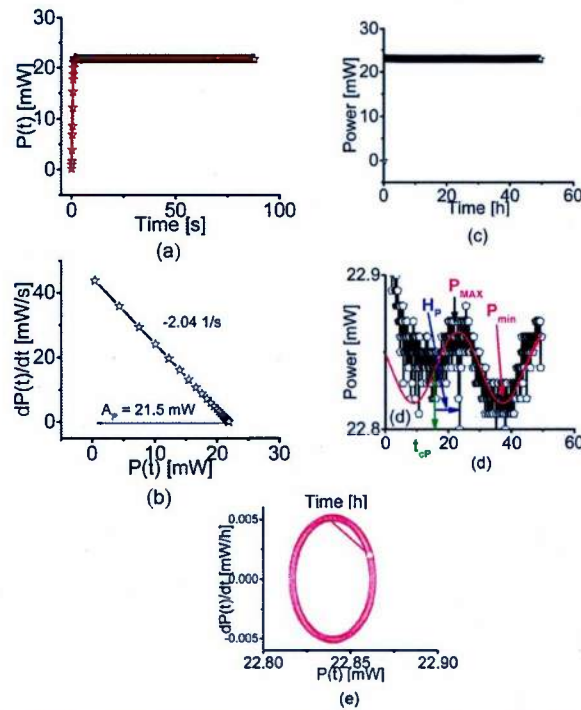
Figure 2. (a) Exponential rise, as in Equation (5), of the power $P(t)$ versus time of the IR radiation emitted by the globar source in the 100 seconds immediately after starting the illumination of the power-meter sensor; (b) Graph of $\left(\Delta P(t), \dfrac{dP(t)}{dt} \right)$ in the same time interval of (a) reporting the slope and amplitude A_P; (c) The power $P(t)$ in the 50 hours after starting the illumination of the power-meter sensor; (d) Same as (c), with the vertical scale expanded to highlight the sinusoidal instability region fitted with Equation (6). The zero of the time-scale coincides with the start of the illumination with the IR radiation. The parameters t_{cP} and H_P are labeled; (e) Graph of $\left(\Delta P(t), \dfrac{dP(t)}{dt} \right)$ in the 50 hours after starting the illumination of the power-meter sensor.

$$P(t) = P_0 e^{-\frac{t}{\tau_P}} + P_f, \tag{5}$$

where P_0 is the offset, P_f the final value, and τ_P the time constant. Typical values of these parameters are reported in **Table 2**. The slope of the $\left(P(t), \frac{dP(t)}{dt}\right)$ graph in **Figure 2(b)** is negative, indicating the evolution of $P(t)$ toward a stable fixed point [22]. The rate of increase of $P(t)$, *i.e.* the absolute value of the slope of the $\left(P(t), \frac{dP(t)}{dt}\right)$ graph, is $\rho_P = 2.04\ \text{s}^{-1}$. The amplitude A_P of $P(t)$, *i.e.* the magnitude of the interval along the horizontal scale of the $\left(P(t), \frac{dP(t)}{dt}\right)$ graph in **Figure 2(b)**, is 21.5 mW. In the 50 hours after starting the illumination of the power-meter sensor, the power $P(t)$, shown **Figure 2(c)**, reaches a plateau. However, in multiple data sets, we always observe that $P(t)$ undergoes small sinusoidal instabilities shown in **Figure 2(d)** in which the vertical scale has been expanded. The instability, due to small periodic fluctuations in the closed sample compartment, can be fitted with:

$$P(t) = P_{off} + P_{osc} \sin\left(\frac{t - t_{cP}}{H_P}\right), \tag{6}$$

where P_{off} and P_{osc} are the offset value and half of the separation between P_{MAX} and P_{min}, respectively. The critical time t_{cP} is the point in time in which $P(t)$ reaches $P_{\text{min}} + P_{osc}$, while H_P is the amount of time necessary to move $P(t)$ from $P_{\text{min}} + P_{osc}$ to P_{MAX} (practically, 1/4 of the period of the sinusoidal function). The typical values of P_{off}, P_{osc}, t_{cP}, and H_P are reported in **Table 2**, labelled in **Figure 2(d)**, and were obtained by placing the zero of the time-scale at the start of the illumination. The instability in $P(t)$ is small, as inferred from $P_{off}/P_{osc} \approx 10^3$. The $\left(P(t), \frac{dP(t)}{dt}\right)$ graph, shown in **Figure 2(e)**, highlights a periodic behavior with frequency $v_P = 1/4H_P \cong 2 \times 10^{-5}$ Hz! We observe the sinusoidal instability of $P(t)$, which modulates the amplitudes of the electric E and magnetic H fields of the IR radiation, to persist beyond the 50 h time interval in **Figure 2(d)**.

b) Action of the IR radiation on $\sigma(r,t)$

We observed that the power $P(t)$ of the IR radiation rises exponentially obeying Equation (5) at the start of the illumination, and exhibits a sinusoidal instability in the 50 hours thereafter. For the entire time span, we hypothesize that the IR radiation transfers energy, through electric contribution ΔE_{el}, to the surface density

Table 2. (Top rows) Fitting parameters P_0, P_f, and τ_P of the IR power $P(t) = P_0 e^{-\frac{t}{\tau_P}} + P_f$ in Equation (5) in the 100 seconds immediately following the start of the illumination of the power-meter sensor with IR radiation from the globar source. The rate of increase of the power (ρ_P), and the amplitude A_P in this time interval, derived from the $\left(P(t), \frac{dP(t)}{dt}\right)$ graph in **Figure 2(b)**, are also reported. (Bottom rows) Typical values of the P_{off}, P_{osc}, t_{cP}, and H_P of the sinusoidal instability $P(t) = P_{off} + P_{osc} \sin\left(\frac{t - t_{cP}}{H_P}\right)$ in Equation (6) of the IR power $P(t)$ in the 50 hours following the start of the illumination of the power-meter sensor with IR radiation from the globar source. The parameters t_{cP} and H_P are labelled in **Figure 2(d)**. The unit for time in the bottom rows of this table is the hour ([h]).

Time interval	P_0 [mW]	P_f [mW]	τ_P [s]	ρ_P [s⁻¹]	A_P [mW]
0 - 100 s	−21.9	21.9	0.5	2.04	21.5
Time interval	P_{off} [mW]	P_{osc} [mW]	H_P [h]	t_{cP} [h]	-
0 - 50 h	21.7 ± 0.7	0.05 ± 0.03	4.0 ± 0.5	16 ± 2	-

$\sigma(r,t)$ of the electrons on the illuminated Cu plate of the PG device, and contributes to producing $\Delta V(t)$ through the E and H fields (electric contribution) and $\Delta T(t)$ (entropic contribution). To prove that a link exists between $P(t)$ and $\Delta V(t)$, possibly also between $P(t)$ and $\Delta T(t)$, we sketch the behavior of $\sigma(r,t)$ and relate it to the observed $P(t)$, $\Delta V(t)$, and $\Delta T(t)$.

To sketch $\sigma(r,t)$, we hypothesize that, while hitting the surface of the Cu plate, the IR radiation modulates the electric field E through the sinusoidal instability of the IR power $P(t) = a\,|S(t)| = a\,|E(t) \times H(t)|$. In turn, E and its modulation act on the electrons of the Cu plate with force $f = eE$, where e is the electron's charge. As in the photoelectric effect [3], f displaces the electrons away from the location in which the IR radiation impinges on the Cu plate, locally decreasing their surface density such that $\sigma(r,t) \propto 1/P(t)$. However, unlike in the photoelectric effect, f does not kick the electrons out of the Cu plate. In this process, $\sigma(r,t)$ varies in time t as well as in space r, *i.e.* the 2-dimensional (2D) surface of the Cu plate. To allow us versatility in choosing reference system, orientation and phase, we represent the 2D space variable r as the complex variable $z = r_x + ir_y$, where i is the imaginary unit. This choice resembles that adopted to describe light polarization through Jones matrices [23]-[25]. Thus, $z = \begin{bmatrix} r_x \\ r_y \end{bmatrix} = \begin{bmatrix} r_{0x}e^{i\varphi_x} \\ r_{0y}e^{i\varphi_y} \end{bmatrix} = \begin{bmatrix} r_a + ir_b \\ r_c + ir_d \end{bmatrix}$. All possible rotations of the reference system, phases, and positions in the 2D plane can be obtained by selecting magnitude and sign of r_a, r_b, r_c, and r_d.

With this choice of z, upon starting the illumination, we picture $\sigma(z,t)$ to exponentially decrease according to $\sigma(z,t) = RE\left(\left|\sigma_0\right|e^{\frac{-t}{\tau_\sigma} + (r_x + ir_y)k + \varphi} - \left|\sigma_f\right|\right)$, where σ_0 and σ_f are the initial and final surface electron densities, τ_σ the time constant, k a vector with units of inverse length, and φ an arbitrary phase. We note that the exponential behavior is modulated by the oscillatory function $e^{ir_y k}$.

In the subsequent 30 hours, from Equation (6) we expect $\sigma(z,t)$ to undergo a slow variation in time such that $\sigma(z,t) \propto 1/P(t) \propto 1\Big/ \sin\left(\dfrac{t - t_{cP}}{H_P}\right)$, where the sine function has the frequency $v_P = 1/4H_P$ derived in Section 3(a). With the choice of z discussed above, and utilizing the laws of trigonometric functions for complex variables, we obtain:

$$\sigma(z,t) \propto RE\left(\frac{1}{\sin(z,t)}\right) = RE\left(\frac{1}{\sin(r_x + ir_y, t)}\right) = \frac{1}{\sin(r_x,t)\cosh(r_y,t)} = \frac{\operatorname{sech}(r_y,t)}{\sin(r_x,t)} = \frac{\operatorname{sech}\left(\dfrac{v_y t - v_y t_{\sigma y}}{L_y}\right)}{\sin\left(\dfrac{v_x t - v_x t_{\sigma x}}{L_x}\right)} \tag{7}$$

Here, v_x and v_y are the instability's propagation velocities along the x and y directions; L_x and L_y are the lengths of the Cu plate along x and y; finally, $t_{\sigma x}$ and $t_{\sigma y}$ are the critical times of the surface electron density's instability along x and y. Considering σ_{off} and σ_{osc}, the equilibrium electron density and its deviation from equilibrium, respectively, we obtain $\sigma(z,t) = \sigma_{off} + \sigma_{osc}\left(\dfrac{\operatorname{sech}\left(\dfrac{v_y t - v_y t_{\sigma y}}{L_y}\right)}{\sin\left(\dfrac{v_x t - v_x t_{\sigma x}}{L_x}\right)}\right)$. The 2D space variable z, therefore unveils a hyperbolic instability in $\sigma(z,t)$ modulated by a sine function.

While $\sigma(z,t)$ requires a spatiotemporal set of variables, the functions $\Delta V(t)$, $T_{IR}(t)$, $T_{no-IR}(t)$, and $\Delta T(t)$ are only time-dependent. To decouple z from the effects of $\sigma(z,t)$ on $\Delta V(t)$, $T_{IR}(t)$, $T_{no-IR}(t)$, and $\Delta T(t)$, and allow time t to be the only effective variable, we integrate $\sigma(z,t)$ over the surface area a of the Cu plate as $\int_o \sigma(z,t)\,\mathrm{d}z$. Because of the capacitor-type structure of the PG device, with overall capacitance C, we expect $\Delta V(t) = \dfrac{a\int_o \sigma(z,t)\,\mathrm{d}z}{C}$. This integration causes the loss of correlation between the phase of

$P(t)$ and $\Delta V(t)$. In the 30 hours after starting the illumination, since $1/\sin(r_x,t) > 1$ where $|\sin(r_x,t)| \neq 0$, from Equation (7) we expect the $\mathrm{sech}(r_y,t)$ function to determine the behavior in time of $\Delta V(t)$. We also envision the capacitor-type structure of the PG device to affect $T_{IR}(t)$ and $T_{no-IR}(t)$, while leaving $\Delta T(t)$ constant.

Summarizing, we expect $\Delta V(t)$ to obey an exponential behavior in the first minutes after starting the illumination, and to exhibit a hyperbolic-secant-type of instability in the 30 hours thereafter, with no phase relationship with $P(t)$, no periodic behavior, and with $\Delta T(t)$ constant. We are currently exploring this hypothesis further numerically, which will be the focus of future work.

c) Behavior of $\Delta V(t)$ and $\Delta T(t)$ in the 400 seconds after starting the illumination

The voltage difference $\Delta V(t)$ and temperature difference $\Delta T(t)$ in the 400 seconds after starting the illumination of the PG device with IR radiation are pictured in **Figure 3** and **Figure 4** for the *away* and the *toward* architectures. We find that the voltage difference $\Delta V(t)$ in **Figure 3(a)** and **Figure 3(d)** fits a sum of exponential functions:

$$\Delta V(t) = \sum_{i=1}^{N} \left(\Delta V_{0i} e^{-\frac{t}{\tau_i}} + \Delta V_{fi} \right), \qquad (8)$$

where the ΔV_{0i} and ΔV_{fi} terms are the initial and final voltage differences, and the τ_i terms are the time constants. These parameters and the number of summands N are summarized in **Table 3**. In both the *away* and the *toward* architectures, the electric contribution is related to the summand with $N = 1$ and $\tau_1 = 3.8\,\mathrm{s}$. The
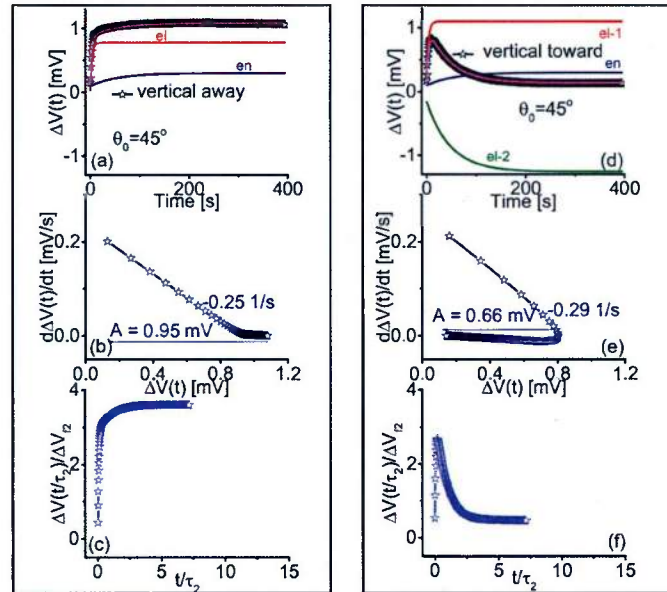

Figure 3. Panels (a), (b), and (c) correspond to the *away* architecture and refer to the 400 seconds immediately following the start the illumination of the PG device with IR radiation. (a) Voltage difference $\Delta V(t)$ with fitting curves obeying Equation (8) highlighting the summands related to the electric (el) and the entropic (en) contributions; (b) Graph of $\left(\Delta V(t), \dfrac{\mathrm{d}\Delta V(t)}{\mathrm{d}t} \right)$ obtained from the fitting parameters in **Table 3**, reporting the slope and amplitude A; (c) Dimensionless voltage $\widetilde{\Delta V(\mathrm{T})} = \Delta V(t)/\Delta V_{f2}$ as in Equation (9). Panels (d), (e), and (f) report the voltage difference $\Delta V(t)$, the $\left(\Delta V(t), \dfrac{\mathrm{d}\Delta V(t)}{\mathrm{d}t} \right)$ graph with slope and amplitude A, and the dimensionless voltage $\widetilde{\Delta V(\mathrm{T})} = \Delta V(t)/\Delta V_{f2}$, respectively, for the *toward* architecture in the 400 seconds immediately following the start the illumination of the PG device with IR radiation. Panel (d) highlights the two summands related to the electric (el-1 and el-2) contributions, and the summand related to the entropic (en) contribution.

entropic contribution is related to the summand with larger time constant, $\tau_2 = 55\,\text{s}$, and is labeled with $N = 2$. This association is justified because $\tau_2 = 55\,\text{s}$ is of the same order of magnitude of $\tau_{T1} = 30\,\text{s}$ for the temperature difference $\Delta T(t)$ in both architectures, as can be seen in **Table 3**, and further in Appendix-1. The summand with $N = 3$, detected only in the *toward* architecture, is related to an electric contribution because the "decay" in $\Delta V(t)$, shown in **Figure 3(d)**, is absent in the corresponding $\Delta T(t)$ in **Figure 4(c)**. We claim that the summand with $N = 3$ causes the "decay" in $\Delta V(t)$ shown in **Figure 3(d)** because of the non-continuity of the Cu plate opposite to the IR radiation illustrated in **Figure 1(b)**. The large value of $\Delta V_{03} = 1.1\,\text{mV}$ signals that the *toward* architecture tries to avoid the "decay" by pumping up the voltage production.

The rates of increase of $\Delta V(t)$ ($\rho_{\Delta V}$) in the initial linear regime of the $\left(\Delta V(t), \dfrac{d\Delta V(t)}{dt}\right)$ graph in **Figure 3(b)** and **Figure 3(e)**, are $\rho_{\Delta V} = 0.25\,\text{s}^{-1}$ in the *away* architecture, and $\rho_{\Delta V} = 0.29\,\text{s}^{-1}$ in the *toward* architecture. The amplitudes A, also derived from **Figure 3(b)** and **Figure 3(e)**, are 0.95 mV and 0.66 mV in the *away* and the *toward* architectures, respectively.

Table 3. Fitting parameters τ_i, ΔV_{0i}, and ΔV_{fi} of the voltage difference $\Delta V(t)$ in: $\Delta V(t) = \sum\limits_{i=1}^{N}\left(\Delta V_{0i}\,e^{-\frac{t}{\tau_i}} + \Delta V_{fi}\right)$, Equation (8) (top rows) and τ_{Ti}, ΔT_{0i}, and ΔT_{fi} of the temperature difference $\Delta T(t)$ in $\Delta T(t) = \sum\limits_{i=1}^{M}\left(\Delta T_{0i}\,e^{-\frac{t}{\tau_{Ti}}} + \Delta T_{fi}\right)$, Equation (10) (bottom rows) in the *away* and *toward* architectures in the 400 seconds immediately following the start of the illumination of the PG device with IR radiation. The corresponding experimental data are shown in **Figure 3(a)** and **Figure 3(d)**, and **Figure 4(a)** and **Figure 4(c)**. The indexes N and M indicate the number of summands in Equations (8) and (10), respectively. The relationship of the summands with either the electric or the entropic contribution is highlighted.

| Away ΔV; $N = 2$	Figure 3(a): $N = 1$, electric	Figure 3(a): $N = 2$, entropic	-
	$\tau_1 = 3.8\,\text{s}$	$\tau_2 = 55.0\,\text{s}$	-
	$\Delta V_{01} = -0.75\,\text{mV}$	$\Delta V_{02} = -0.20\,\text{mV}$	-
	$\Delta V_{f1} = 0.78\,\text{mV}$	$\Delta V_{f2} = 0.30\,\text{mV}$	-
Toward ΔV; $N = 3$	Figure 3(d): $N = 1$, electric	Figure 3(d): $N = 2$, entropic	Figure 3(d): $N = 3$ electric
	$\tau_1 = 3.8\,\text{s}$	$\tau_2 = 55.0\,\text{s}$	$\tau_3 = 48.0\,\text{s}$
	$\Delta V_{01} = -0.88\,\text{mV}$	$\Delta V_{02} = -0.20\,\text{mV}$	$\Delta V_{03} = 1.10\,\text{mV}$
	$\Delta V_{f1} = 1.10\,\text{mV}$	$\Delta V_{f2} = 0.30\,\text{mV}$	$\Delta V_{f3} = -1.26\,\text{mV}$
Away ΔT; $M = 1$	Figure 4(a): $M = 1$, entropic	-	-
	$\tau_{T1} = 30.0\,\text{s}$	-	-
	$\Delta T_{01} = -0.135°\text{C}$	-	-
	$\Delta T_{f1} = -0.26°\text{C}$	-	-
Toward ΔT; $M = 2$	Figure 4(c): $M = 1$, entropic	Figure 4(c): $M = 2$, entropic	-
	$\tau_{T1} = 30.0\,\text{s}$	$\tau_{T2} = 2000.0\,\text{s}$	-
	$\Delta T_{01} = -0.136°\text{C}$	$\Delta T_{02} = -0.36°\text{C}$	-
	$\Delta T_{f1} = -0.25°\text{C}$	$\Delta T_{f2} = 0.20°\text{C}$	-
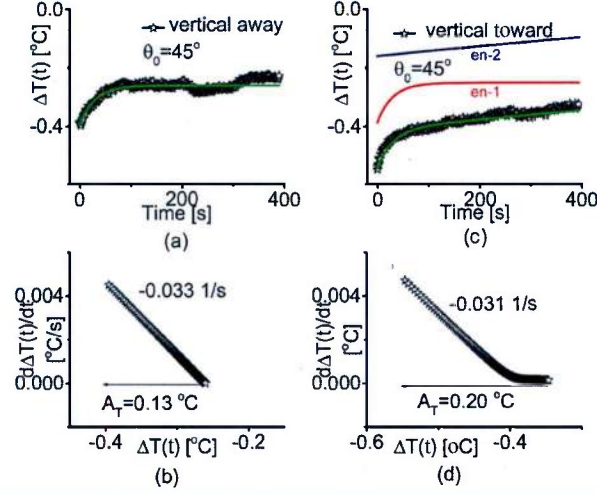
Figure 4. Panels (a) and (b) correspond to the *away* architecture and refer to the 400 seconds immediately following the start of the illumination of the PG device with IR radiation. (a) Temperature difference $\Delta T(t)$ with exponential behavior as in Equation (10); (b) Graph of $\left(\Delta T(t), \dfrac{d\Delta T(t)}{dt}\right)$ obtained from fitting parameters in **Table 3**, reporting the slope and amplitude A_T. Panels (c) and (d) report the temperature difference $\Delta T(t)$ and the $\left(\Delta T(t), \dfrac{d\Delta T(t)}{dt}\right)$ graph with slope and amplitude A_T for the *toward* architecture in the 400 seconds immediately following the start the illumination of the PG device with IR radiation. Panel (c) highlights the two summands related to the entropic (en-1 and en-2) contribution.

As with the power $P(t)$, the voltage difference $\Delta V(t)$ produced by the PG device also rises exponentially in the first few minutes after starting the illumination. However, $\rho_{\Delta V}=0.25$ and $0.29\,\text{s}^{-1}$ are one order of magnitude smaller than $\rho_P=2.04\,\text{s}^{-1}$ for the power $P(t)$ shown in **Figure 2(b)**. We ascribe this discrepancy to the activation process occurring in the PG device to start the $\Delta V(t)$ production.

We capture the relative behavior of the electric and the entropic contributions to the generation of $\Delta V(t)$ using the dimensionless voltage $\widetilde{\Delta V(\text{T})}=\Delta V(t)/\Delta V_{f2}$ [22], pictured in **Figure 3(c)** and **Figure 3(f)**, and derived from Equation (8) and its parameters in **Table 3** as follows:

$$\widetilde{\Delta V(\text{T})}=\sum_{i=1}^{N}\left(\frac{\Delta V_{0i}}{\Delta V_{f2}}e^{-\text{T}\frac{\tau_2}{\tau_i}}+\frac{\Delta V_{fi}}{\Delta V_{f2}}\right). \tag{9}$$

Here, the term $\text{T}=t/\tau_2$ is the dimensionless time [22], while $r_{0i}=\Delta V_{0i}/\Delta V_{f2}$ and $r_{fi}=\Delta V_{fi}/\Delta V_{f2}$ are dimensionless voltage parameters. We performed the normalization with respect to the slower summand, *i.e.* the one related to the entropic contribution with $N=2$. Such a choice leads us to observe an evolution of $\widetilde{\Delta V(\text{T})}$ in **Figure 3(c)** and **Figure 3(f)** on a similar T-scale in both the *away* and the *toward* architectures, signifying that the dynamics is not affected by the architecture. On the other hand, from the plateau value at $\widetilde{\Delta V(\text{T})}\approx 4$ in the *away* architecture, we infer that the summands related to the electric and entropic contributions add one to the other, with the former prevailing over the latter because of $r_{f1}=\Delta V_{f1}/\Delta V_{f2}=2.6>1$. On the contrary, from the plateau value at $\widetilde{\Delta V(\text{T})}<1$ in the *toward* architecture, we conclude that the two summands related to the electric contributions with $N=1$ and 3 almost annihilate one another, while the summand related to the entropic contribution survives in the long term.

The temperature difference $\Delta T(t)$, shown in **Figure 4(a)** and **Figure 4(c)**, surprisingly exhibits negative values, indicating that $T_{IR}(t)<T_{no-IR}(t)$. This behavior is typical when the PG device faces the IR radiation with the Cu plate. Nevertheless, we find that the temperature difference $\Delta T(t)$ rises exponentially as follows:

$$\Delta T(t) = \sum_{i=1}^{M} \left(\Delta T_{0i} e^{-\frac{t}{\tau_{Ti}}} + \Delta T_{fi} \right), \tag{10}$$

where ΔT_{0i} and ΔT_{fi} are the initial and final temperature differences, respectively, and the τ_{Ti} terms are the time constants. These time constants reflect the fact that generally $T_{IR}(t)$ rises faster than $T_{no-IR}(t)$. The parameters and the number of summands M, all related to the entropic contribution, are summarized in **Table 3**. We observe that $1 \leq M \leq 2$, and that summands similar to that with $M = 2$ (rarely detected) in the *toward* architecture in **Figure 4(c)** exhibit an extremely large time constant of $\tau_{T2} = 2000\,\text{s}$. We also note that no "decay" appears for $\Delta T(t)$ in the *toward* architecture in **Figure 4(c)**, as opposed to the corresponding voltage difference $\Delta V(t)$ in **Figure 3(d)**.

The slopes of the initial linear regimes in the $\left(\Delta T(t), \dfrac{\mathrm{d}\Delta T(t)}{\mathrm{d}t} \right)$ graphs, displayed in **Figure 4(b)** and **Figure 4(d)**, are negative, as those of $P(t)$ in **Figure 2(b)**, and $\Delta V(t)$ in **Figure 3(b)** and **Figure 3(e)**. The rates of increase of $\Delta T(t)$ are $\rho_{\Delta T} = 0.033\,\text{s}^{-1}$ and $\rho_{\Delta T} = 0.031\,\text{s}^{-1}$ in the *away* and *toward* architectures, respectively. The corresponding amplitudes A_T are 0.13°C and 0.20°C in the *away* and the *toward* architectures, respectively. The ratio $R = \Delta(\Delta V)/\Delta(\Delta T)$ between the jump in voltage $(\Delta(\Delta V))$ and temperature difference $(\Delta(\Delta T))$ in the *away* architecture is $R = 7.31\,\text{mV/°C}$.

Overall, **Figure 3** and **Figure 4** suggest that $\Delta V(t)$ and $\Delta T(t)$ evolve independently, with different rates of increase such that $\rho_{\Delta V} \gg \rho_{\Delta T}$. The electric contribution affects only $\Delta V(t)$. Thus, we conclude that the electric and entropic contributions in the interaction of IR radiation with a PG device are decoupled. To further support this conclusion, in Appendix-1 we will compare the trends of $\rho_{\Delta V}$, $\rho_{\Delta T}$, $R = \Delta(\Delta V)/\Delta(\Delta T)$, and the values of $\Delta(\Delta V)$ upon activating the PG device with IR radiation, as done so far, and conductive heat transfer from a 100 Ω resistor and a 0.02 A current. Only the entropic contribution is activated in this case because the produced power of 0.04 W, corresponding to a temperature of ≈ 24°C on the PG device, is too low to produce significant blackbody radiation to trigger the electric contribution.

d) Behavior of $\Delta V(t)$ and $\Delta T(t)$ in the 30 hours after starting the illumination

The voltage difference $\Delta V(t)$ and temperature difference $\Delta T(t)$ evolve in the 30 hours after starting the illumination of the PG device as pictured in **Figure 5** and **Figure 6**. We observed one possible behavior in **Figure 5**, which displays the data collected with the *toward* architecture. The voltage difference $\Delta V(t)$ in **Figure 5(a)**, exhibits an instability around the 20$^\text{th}$ hour. No instability is detected in $\Delta T(t)$ in **Figure 5(b)**, which is almost flat. The same instability affecting $\Delta V(t)$, however, is revealed in $T_{IR}(t)$ and $T_{no-IR}(t)$, displayed in **Figure 5(c)** and **Figure 5(d)**, respectively. This finding suggests that a strong correlation exists among $\Delta V(t)$, $T_{IR}(t)$ and $T_{no-IR}(t)$, which we ascribe to the capacitor-type of structure of the PG device, as predicted in Section 3(b).

We observed another possible behavior in **Figure 6**, displaying data collected with the *away* architecture. In this case, $\Delta V(t)$, shown in **Figure 6(a)**, exhibits an instability around the 12$^\text{th}$ hour which is uncorrelated with the trends occurring in $T_{IR}(t)$ and $T_{no-IR}(t)$. The lack of correlation highlights the lack of coupling between the electric and the entropic contributions. Since the trends of the two temperatures are identical, we show only $T_{IR}(t)$ in **Figure 6(b)**. We omit to display $\Delta T(t)$, which is flat as hypothesized in Section 3(b). The instability of $\Delta V(t)$ in **Figure 6(a)** is non-periodic, as predicted in Section 3(b). Thus, to find a suitable fitting function, we recall the hypothesis in Section 3(b) where we pictured the time-dependence of $\Delta V(t)$ in **Figure 6(a)** as captured by a hyperbolic secant function with no phase relationship with $P(t)$ and no sinusoidal periodicity. Thus, we propose:

$$\Delta V(t) = \Delta V_{off} + \Delta V_{osc} \operatorname{sech}\left(\frac{t - t_c}{H} \right). \tag{11}$$

In this expression, ΔV_{off} and ΔV_{osc} are the offset and amplitude of the departure of $\Delta V(t)$ from the offset, respectively. The positive or negative sign of ΔV_{osc} corresponds to a downward or upward concavity, respectively, of the instability. The critical time t_c is the instant in which the maximum $|\Delta V_{osc}|$ value is achieved. Finally, the term H indicates the half width at half maximum (HWHM), or minimum (depending upon the sign of ΔV_{osc}) of the instability. The magnitude of ΔV_{off} corresponds to the long term equilibrium voltage
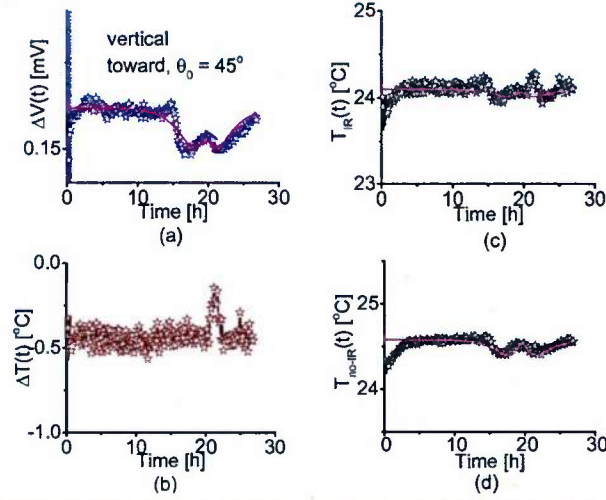
Figure 5. Panels (a), (b), (c), and (d) correspond to data collected from the *toward* architecture in the whole time span of about 30 hours following the start of the illumination of the PG device with IR radiation. (a) Voltage difference $\Delta V(t)$. (b) Temperature difference $\Delta T(t)$. Temperatures $T_{IR}(t)$ (c) and $T_{no-IR}(t)$ (d) of the illuminated and non-illuminated faces, respectively, of the PG device. The zero of the time-scale coincides with the start of the illumination with the IR radiation, and the unit for time is the hour ([h]).

ΔV_{f2} reported in **Table 3**. The typical values of ΔV_{off}, ΔV_{osc}, t_c, and H are reported in **Table 4**, labelled in **Figure 6(a)**, and were obtained by placing the zero of the time-scale at the start of the illumination. We highlight that, since $T_{IR}(t)$ in **Figure 6(b)** does not peak at t_c, it does not correlate with the behavior in time of $\Delta V(t)$. The instability in $\Delta V(t)$ is evidenced in the $\left(\Delta V(t), \dfrac{\mathrm{d}\Delta V(t)}{\mathrm{d}t} \right)$ graph in **Figure 6(c)**, where stable and unstable fixed points [20] alternate in a complex fashion without periodicity.

Since the time-dependence is enclosed in a hyperbolic secant function, we name the instability in $\Delta V(t)$ in Equation (11) and **Figure 6(a)** as hyperbolic instability. We establish the lack of correlation between $\Delta V(t)$, on one hand, and $T_{IR}(t)$ and $T_{no-IR}(t)$ on the other, as the criterion to identify such instability. Since the hyperbolic instability in $\Delta V(t)$ is absent in $\Delta T(t)$, as expected from Section 3(b), we relate the instability to the sole electric contribution.

e) Correlation between $P(t)$ and $\Delta V(t)$ in the 30 hours after starting the illumination

Here we highlight the correlations existing between the power $P(t)$ and the voltage difference $\Delta V(t)$ to further support the choice of the fitting function in Equation (11) for $\Delta V(t)$ based on the hypothesis highlighted in Section 3(b).

1) The average H_P of the power $P(t)$ in **Table 2** is $4.0 \pm 0.5\,\text{h}$, about twice the value of 1.82 h reported in **Table 4** for H of $\Delta V(t)$.

2) The instabilities in $P(t)$ and $\Delta V(t)$ are both small: the former is $P_{off}/P_{osc} \approx 10^3$, while the latter is $\Delta V_{off}/\Delta V_{osc} \approx 10/10^2$.

3) The t_c term in **Table 4** is found at 11.65 h, which is reasonably close to the average t_{cP} at 16 ± 2 in **Table 2**.

These observations further support our hypothesis in Section 3(b) relating the sinusoidal instability of $P(t)$ to $\Delta V(t)$ through $\sigma(z,t)$ on the Cu plate. In Appendix-2 we will show that the hyperbolic instability in $\Delta V(t)$, selected according to the criterion established in Section 3(d), occurs frequently in our observations. We will provide further evidence of the link between t_c and t_{cP}. Finally, we will prove the lack of phase relationship between $P(t)$ and $\Delta V(t)$ through lack of predictability of the sign of the amplitude ΔV_{osc} of the departure of $\Delta V(t)$ from equilibrium.

f) The nonlinearity of the hyperbolic instability in $\Delta V(t)$

We found that Equation (11), used to fit the hyperbolic instability in $\Delta V(t)$ in the 30 hours after starting the
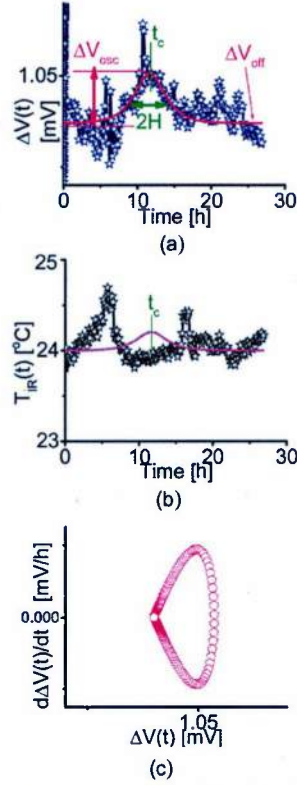
(a)

(b)

(c)

Figure 6. Panels (a), (b), and (c) correspond to data collected from the *away* architecture in the whole time span of about 30 hours following the start of the illumination of the PG device with IR radiation. (a) Voltage difference $\Delta V(t)$ exhibiting the hyperbolic instability obeying Equation (11). The parameters ΔV_{off}, ΔV_{osc}, t_c, and H, reported in **Table 4**, are labelled. (b) Temperature $T_{IR}(t)$ of the face of the PG device illuminated by the IR radiation, and exhibiting no correlation with the hyperbolic instability in $\Delta V(t)$ highlighted by t_c. (c) Graph of $\left(\Delta V(t), \dfrac{d\Delta V(t)}{dt} \right)$ obtained using the parameters in **Table 4**. The zero of the time-scale coincides with the start of the illumination with the IR radiation, and the unit for time is the hour ([h]).

Table 4. Parameters of $\Delta V(t) = \Delta V_{off} + \Delta V_{osc} \operatorname{sech}\left(\dfrac{t-t_c}{H} \right)$ in Equation (11) used to fit the voltage difference $\Delta V(t)$ in **Figure 6(a)** collected from the *away* architecture in the time interval of about 30 hours following the start the illumination of the PG device with IR radiation. The parameters ΔV_{off}, ΔV_{osc}, t_c, and H are labeled in **Figure 6(a)**.

Away	ΔV_{off} [mV]	ΔV_{osc} [mV]	t_c [h]	H [h]
	1.037	0.0137	11.65	1.82

illumination of the PG device with IR radiation, can be a solution of the equation:

$$\sigma \Delta V(t) \frac{\partial \Delta V(t)}{\partial t} + \varsigma \frac{\partial^3 \Delta V(t)}{\partial t^3} = 0 . \tag{12}$$

Equation (12) is nonlinear because of the 3rd order partial differential of $\Delta V(t)$ with respect to time t. The equation resembles the Korteweg-de Vries (KdV) equation [26] [27] after eliminating the space-dependence, and flipping the space variable with time t. In order for $\Delta V(t)$ in Equation (11) to be a solution of Equation (12), we select the σ and ς coefficients by rewriting Equation (12) as:

$$\Omega \Delta V(t) \frac{\partial \Delta V(t)}{\partial t} + \frac{\partial^3 \Delta V(t)}{\partial t^3} = 0.$$ (13)

By substituting Equation (11) into Equation (13), we obtain:

$$\Omega(t) = \frac{1}{H^2} \left(\frac{5\text{sech}\left(\frac{t-t_c}{H}\right)^2 - \tan\left(\frac{t-t_c}{H}\right)^2}{\Delta V_{osc}\text{sech}\left(\frac{t-t_c}{H}\right) + \Delta V_{off}} \right).$$ (14)

The time-dependent coefficient $\Omega(t) = \sigma(t)/\varsigma(t)$ of Equation (13) stands for nonlinear effects [26], and infers that a complex dynamics is hidden in the hyperbolic instability of $\Delta V(t)$ [28] [29]. In **Figure 7** we graph $\Omega(t)$ using the parameters reported in **Table 4** for the *away* architecture. Despite the complexity of Equation (14), $\Omega(t)$ appears surprisingly simple, correlates with the time-scale of the hyperbolic instability in $\Delta V(t)$, and peaks at t_c. Furthermore, we determined the physical units of $\Omega(t)$ to be $1/h^2 (1/\text{mV})$ (where h indicates the hour), which suggests that $\Omega(t)$ could be interpreted as the change in time of the rate of $1/\Delta V(t)$, or simply, the "acceleration" of the inverse voltage. Such identification points out the existence of nonlinear "forces" that continuously push and slow down the changes in $\Delta V(t)$. We plan on further investigating this topic.

4. Summary and Significance

We identify and decouple an electric and an entropic contribution to energy transfer from low power infrared radiation to a power generator device. The electric contribution is related to the effects of the electric E and magnetic H fields in the infrared radiation and is detected through the voltage produced by the power generator device. The entropic contribution is mainly related to the temperature difference between the faces of the device. Two observations enable us to decouple the electric and entropic contributions. First, the electric contribution imparts faster rates of increase of the voltage difference $\Delta V(t)$ produced by the power generator device immediately after starting the illumination with infrared radiation. Second, the electric contribution generates a hyperbolic instability in the 30 hours after starting the illumination. The entropic contribution changes slowly and simply reflects the relative delay with which the two faces of the power generator device respond to thermal perturbations.

Our preliminary studies suggest that it is important to learn to exploit the electric contribution, because it offers a variety of ways to increase the voltage produced by the power generator device. For example, black-colored gaffer tape on the illuminated face doubles the amount of voltage produced, as discussed in Appendix-1, while the temperature difference, thus the entropic contribution, is not sensitive to the presence of the tape. Our findings are relevant for understanding the mechanisms for harvesting IR radiation, and possibly other electromagnetic radiations, through a power generation device as an alternative energy source.
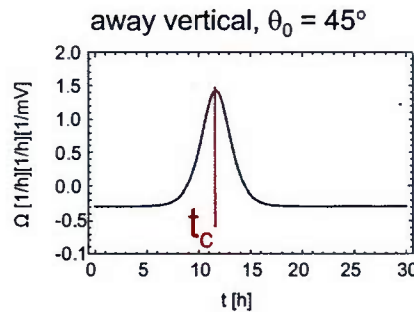

Figure 7. "Acceleration" of the inverse voltage $\Omega(t)$ for the *away* architecture obtained from Equation (14) using the parameters in **Table 4**. The time-dependent coefficient $\Omega(t)$ peaks at t_c, reported in **Table 4**. The unit for time is the hour ([h]).

The future efforts will be devoted to overcome the limitations of the present work: 1) understand the relationship among infrared source power, surface charge density on the power generator, and produced voltage, 2) clarify the behavior of the power generator as a capacitor, and 3) investigate the role of infrared radiation power on the results.

Acknowledgements

References

[1] Christillin, P. (1986) Nuclear Compton Scattering. *Journal of Physics G: Nuclear and Particle Physics*, **12**, 837-851. http://dx.doi.org/10.1088/0305-4616/12/9/008

[2] Siegbahn, K.M. (1981) Electron Spectroscopy for Atoms, Molecules and Condensed Matter. Nobel Lecture, 8 December.

[3] Einstein, A. (1905) Concerning an Heuristic Point of View toward the Emission and Transformation of Light. *Annalen der Physik*, **17**, 132-148. http://dx.doi.org/10.1002/andp.19053220607

[4] Becquerel, E. (1839) Mémoire sur les effets électriques produits sous l'influence des rayons solaires. *Comptes Rendus*, **9**, 561-567.

[5] Burdick, G.A. (1963) Energy Band Structure of Copper. *Physical Review*, **129**, 138-150. http://dx.doi.org/10.1103/PhysRev.129.138

[6] Newnham, R.E., Jang, S.J., Xu, M. and Jones, F. (1991) Fundamental Interaction Mechanisms between Microwaves and Matter. *Ceramic Transactions*, **21**, 51-67.

[7] Kliewer, K.L. and Fuchs, R. (1966) Optical Modes of Vibration in an Ionic Crystal Slab including Retardation. 1. Nonradiative Region. *Physical Review*, **144**, 495-503. http://dx.doi.org/10.1103/PhysRev.144.495

[8] Kliewer, K.L. and Fuchs, R. (1966) Optical Modes of Vibration in an Ionic Crystal Slab including Retardation. II. Radiative Region. *Physical Review*, **150**, 573-588. http://dx.doi.org/10.1103/PhysRev.150.573

[9] Fuchs, R., Kliewer, K.L. and Pardee, W.J. (1966) Optical Properties of an Ionic Crystal Slab. *Physical Review*, **150**, 589-596. http://dx.doi.org/10.1103/PhysRev.150.589

[10] Berreman, D.W. (1963) Infrared Absorption at Longitudinal Optic Frequency in Cubic Crystal Films. *Physical Review*, **130**, 2193-2198. http://dx.doi.org/10.1103/PhysRev.130.2193

[11] Gest, H. (2002) History of the Word Photo Synthesis and Evolution of Its Definition. *Photosynthesis Research*, **73**, 7-10. http://dx.doi.org/10.1023/A:1020419417954

[12] Kuesco, G., Mauer, P.C., Yao, N.Y., Kubo, M., Noh, H.J., Lo, P.K., Park, H. and Lukin, M.D. (2013) Nanometre-Scale Thermometry in a Living Cell. *Nature*, **500**, 54-59. http://dx.doi.org/10.1038/nature12373

[13] Jameson, A.D., Tomaino, J.L., Lee, J.-S., Khitrova, G., Gibbs, H.M., Böttge, C.N., Klettke, A.C., Kira, M. and Koch, S.W. (2014) Direct Measurement of Light-Matter Energy Exchange inside a Microcavity. *Optica*, **1**, 276-280. http://dx.doi.org/10.1364/OPTICA.1.000276

[14] Kumar, A., Low, T., Fung, K.H., Avouris, P. and Fang, N.X. (2015) Tunable Light-Matter Interaction and the Role of Hyperbolicity in Graphene-hBN System. *Nano Letters*, **15**, 3172-3180. http://dx.doi.org/10.1021/acs.nanolett.5b01191

[15] Richter, C.-P., Rajguru, S., Stafford, R. and Stock, S.R. (2013) Radiant Energy during Infrared Neural Stimulation at the Target Structure. *Proceedings of SPIE*, **8565**, Article ID: 85655P. http://dx.doi.org/10.1117/12.2013849

[16] Eisen, D., Janssen, D., Chen, X., Choa, F.-S., Kotsov, D. and Fan, J. (2013) Closing a Venus Flytrap with Electrical and Mid-IR Photon Stimulations. *Proceedings of SPIE*, **8565**, Article ID: 85655I. http://dx.doi.org/10.1117/12.2005351

[17] Tritt, T.M., Böttner, H. and Chen, L. (2008) Thermoelectrics: Direct Solar Thermal Energy Conversion. *MRS Bulletin*, **33**, 366-368. http://dx.doi.org/10.1557/mrs2008.73

[18] Tritt, T.M. (2011) Thermoelectric Phenomena, Materials, and Applications. *Annual Review of Materials Research*, **41**, 433-438. http://dx.doi.org/10.1146/annurev-matsci-062910-100453

[19] Bell, L.E. (2008) Cooling, Heating, Generating Power, and Recovering Waste Heat with Thermoelectric Systems. *Science*, **321**, 1457-1461. http://dx.doi.org/10.1126/science.1158899

[20] Vining, C.B. (2009) An Inconvenient Truth about Thermoelectrics. *Nature Materials*, **8**, 83-85. http://dx.doi.org/10.1038/nmat2361

[21] Schwab, Y., Mann, H.S., Lang, B.N., Lancaster, J.L., Parise, R.J., Vincent-Johnson, A.J. and Scarel, G. (2013) Infrared Power Generation in an Insulated Compartment. *Complexity*, **19**, 44-55. http://dx.doi.org/10.1002/cplx.21484

[22] Strogatz, S.H. (1994) Nonlinear Dynamics and Chaos. Westview Press, Cambridge, MA.

[23] Jones, R.C. (1941) A New Calculus for the Treatment of Optical Systems. I. Description and Discussion of the Calculus. *Journal of the Optical Society of America*, **31**, 488-493. http://dx.doi.org/10.1364/JOSA.31.000488

[24] Jones, R.C. (1941) A New Calculus for the Treatment of Optical Systems. III. The Sohncke Theory of Optical Activity. *Journal of the Optical Society of America*, **31**, 500-503. http://dx.doi.org/10.1364/JOSA.31.000500

[25] Jones, R.C. (1942) A New Calculus for the Treatment of Optical Systems. IV. *Journal of the Optical Society of America*, **32**, 486-493. http://dx.doi.org/10.1364/JOSA.32.000486

[26] Korteweg, D.J. and de Vries, G. (1895) On the Change of Form of Long Waves Advancing in a Rectangular Canal and a New Type of Long Stationary Waves. *Philosophical Magazine Series*, **39**, 422-443. http://dx.doi.org/10.1080/14786449508620739

[27] Smaoui, N. and Zribi, M. (2009) A Finite Dimensional Control of the Dynamics of the Generalized Korteweg-de Vries Burgers Equation. *Applied Mathematics & Information Sciences*, **3**, 207-221.

[28] Jiang, Y., Tian, B., Liu, W.-J., Sun, K. and Qu, Q.-X. (2010) Soliton Solutions for a Variable-Coefficient Korteweg-de Vries Equation in Fluids and Plasmas. *Physica Scripta*, **82**, Article ID: 055008. http://dx.doi.org/10.1088/0031-8949/82/05/055008

[29] Vlieg-Hulstman, M. and Halford, W.D. (1995) Exact Solutions to KdV Equations with Variable Coefficients and/or Nonuniformities. *Computers & Mathematics with Applications*, **29**, 39-47. http://dx.doi.org/10.1016/0898-1221(94)00205-Y

[30] Mann, H.S., Schwab, Y., Lang, B.N., Lancaster, J.L., Parise, R.J. and Scarel, G. (2014) Effective Thermoelectric Power Generation in an Insulated Compartment. *World Journal of Condensed Matter Physics*, **4**, 153-165. http://dx.doi.org/10.4236/wjcmp.2014.43020

Appendix-1

To highlight the effects of the entropic contribution and decouple it from the electric contribution, we collected the voltage difference $\Delta V(t)$ and the temperature difference $\Delta T(t)$ from the PG device activated by conductive heat transfer from a 100 Ω resistor in contact with the surface of the device. A temperature of $\approx 24°C$ was generated by the PG device activated with a B&K Precision 1665 power supply providing 0.02 A and 3.2 V to the resistor. The achieved temperature is of the same order of magnitude as that detected when IR radiation hits the PG device, as can be seen in **Figure 5(c)** and **Figure 5(d)**. We used a PG device 07111-9L31-04B by Custom Thermoelectric Inc. finished with an AlO plate (not with a Cu plate) and, in selected cases, gaffer tape. We placed the sample holders on both sides of the PG device in the *toward* architecture to create a capacitor structure with electrodes on both faces and thus avoid the "decay" in $\Delta V(t)$ shown in **Figure 3(d)**. The experiments investigating the effects of conductive heat transfer were performed in an insulated sample compartment described in Ref. [30]. The PG device was horizontally fixed on the sample holders in all the measurements. When the IR radiation was used to compare the results obtained with conductive heat transfer, the PG device was also positioned horizontally and at an angle of incidence $\theta_0 = 30°$ with respect to the IR radiation. The basic experimental parameters are summarized in **Table 1**.

In the 400 seconds immediately following the start the activation of the PG device by either conductive heat transfer or IR radiation, we measured the rate of increase of $\Delta V(t)$ ($\rho_{\Delta V}$) and $\Delta T(t)$ ($\rho_{\Delta T}$), and the ratio $R = \Delta(\Delta V)/\Delta(\Delta T)$ between the jumps in voltage $(\Delta(\Delta V))$ and temperature difference $(\Delta(\Delta T))$ in the *away* and *toward* architectures. We report the average values of $\rho_{\Delta V}$, $\rho_{\Delta T}$, and R, alongside their uncertainties, in **Figures A1(a)-(c)**, respectively. **Figure A1(a)** indicates that the average $\rho_{\Delta V}$ values obtained by activating the PG device with IR radiation are always larger than those obtained by activating the PG device using conductive heat transfer. **Figure A1(b)** suggests that the average $\rho_{\Delta T}$ values have a common value, independently of the source of activation of the PG device. Moreover, the average $\rho_{\Delta V}$ and $\rho_{\Delta T}$ values are similar when the PG device is activated by conductive heat transfer. In addition, the $\rho_{\Delta T}$ values coincide with those derived from **Figure 4(b)** and **Figure 4(d)**. This finding supports the identification of the contribution to energy transfer with slower rate of increase with the entropic contribution. **Figure A1(c)** shows that, within the errors, the average
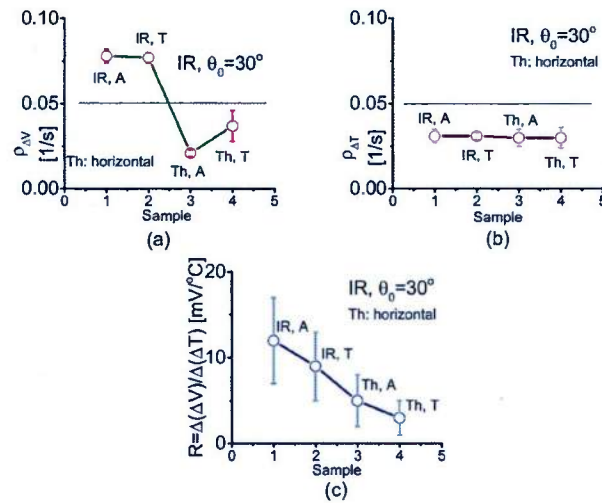

Figure A1. (a) Rate of increase of the voltage difference ($\rho_{\Delta V}$). (b) Rate of increase of the temperature difference ($\rho_{\Delta T}$). (c) Ratio $R = \Delta(\Delta V)/\Delta(\Delta T)$ between the jump in voltage $(\Delta(\Delta V))$ and temperature difference $(\Delta(\Delta T))$. The data were obtained performing measurements in the *away* (*A*) and *toward* (*T*) architectures on a PG device finished with an AlO plate covered with gaffer tape, described in Appendix-1. The results compare data obtained in the 400 seconds immediately following the start the activation of the PG device with IR radiation (IR) or conductive heat transfer (Th) from a 100 Ω resistor. The horizontal line at 0.05 s^{-1} in panels (a) and (b) highlights the level above which only $\rho_{\Delta V}$ values due to IR radiation can be detected. The PG device was horizontally fixed on the sample holders in all the measurements. When the IR radiation was used, the PG device was positioned at an angle of incidence $\theta_0 = 30°$ with respect to the IR radiation.

value of the ratio R is larger when the PG device is activated by IR radiation through the electric contribution.

In the 400 seconds immediately following the start the activation of the PG device by either conductive heat transfer or IR radiation, we also measured the jump in voltage $(\Delta(\Delta V))$ obtained performing measurements on the PG device described above and finished with colored gaffer tape. We performed the measurements for the *away* and *toward* architectures. **Figure A2(a)** displays the magnitude of $\Delta(\Delta V)$ obtained by activating the PG device with conductive heat transfer from a 100 Ω resistor. The observed trends are neither affected by the color nor by the presence of the tape. On the other hand, **Figure A2(b)** shows that the magnitude of $\Delta(\Delta V)$ obtained by activating the PG device with IR radiation, is slightly sensitive to the color of the tape, and exhibits a notice-able drop when the tape is absent. Interestingly, the black-colored tape on the illuminated face of the PG device doubles the magnitude of $\Delta(\Delta V)$ compared to the case without tape. Values of $\Delta(\Delta V)$ above 0.5 mV, repre-sented by the horizontal line in **Figure A2(b)**, can be achieved only with tape present on the illuminated face of the PG device. Thus, we conclude that the tape profoundly affects the capacitor-type behavior of the PG device.

In the time span of about 50 hours following the start of the activation of the PG device with conductive heat transfer from a 100 Ω resistor, the voltage difference $\Delta V(t)$, temperature difference $\Delta T(t)$, and temperatures $T_{hot}(t)$ and $T_{cold}(t)$ of the activated and non-activated faces, respectively, are shown in **Figures A3(a)-(d)**. We collected the particular set of data chosen using the PG device described above, finished with pink-colored gaffer tape, and set-up in the *away* architecture. Nevertheless, **Figure A3** is representative of all the data col-lected in the *away* and *toward* architectures, with tape of all the available colors, and without tape. In all these cases, we observed $\Delta V(t)$, $\Delta T(t)$, $T_{hot}(t)$, and $T_{cold}(t)$ to be featureless and follow the same trends. The trend of $\Delta V(t)$ is symmetric to that of $\Delta T(t)$, $T_{hot}(t)$, and $T_{cold}(t)$. This behavior differs from that observed for the PG device activated by the IR radiation and captured in **Figure 5**. In this case, $\Delta V(t)$ and the tempera-tures $T_{IR}(t)$ and $T_{no-IR}(t)$ of the illuminated and non-illuminated faces are strongly correlated, while $\Delta T(t) = T_{IR}(t) - T_{no-IR}(t)$ is flat and featureless.

The results in **Figures A1-A3**, together with those of **Figures 3-5**, further support that the electric and the en-tropic contribution to energy transfer from low power IR radiation to the PG device are decoupled.

Appendix-2

Figure 6 shows the hyperbolic instability revealed in the voltage difference $\Delta V(t)$ in the time span of about 30 hours following the start of the illumination of the PG device with IR radiation in the *away* architecture. We identify such hyperbolic instability when no correlation is found between $\Delta V(t)$ and the temperatures $T_{IR}(t)$ and $T_{no-IR}(t)$ of the illuminated and non-illuminated faces of the PG device, respectively, and when $\Delta T(t)$ is flat. To demonstrate that hyperbolic instabilities are common in the interaction between IR radiation and a PG device, we collected a set of measurements with the PG device described in Appendix-1. With the AlO plate or
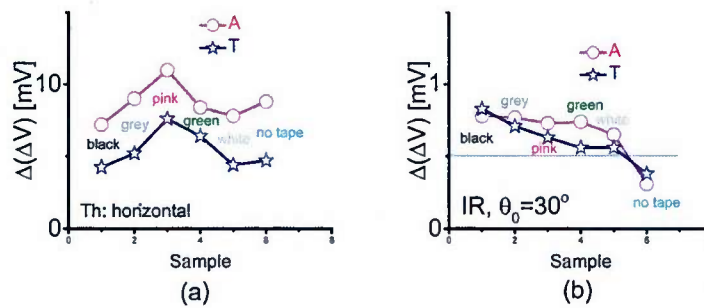

Figure A2. Jump in voltage $(\Delta(\Delta V))$ obtained performing measurements in the *away* (A) and *toward* (T) architectures on a PG device, described in Appendix-1, finished with an AlO plate covered with colored gaffer tape. The results compare data obtained in the 400 seconds immediately following the start the activation of the PG device with (a) conductive heat transfer from a 100 Ω resistor or (b)IR radiation. The PG device was horizontally fixed on the sample holders in all the measure-ments. When the IR radiation was used, the PG device was positioned at an angle of incidence $\theta_0 = 30$ with respect to the IR radiation. The horizontal line at 0.5 mV represents the minimum value of $\Delta(\Delta V)$ that can be obtained only by placing tape on the illuminated face of the PG device.
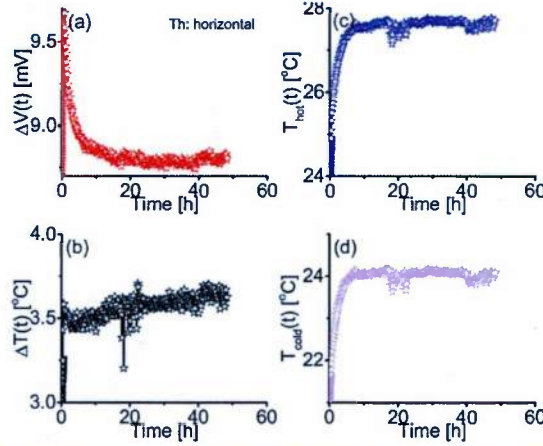
Figure A3. Panels (a), (b), (c), and (d) correspond to data collected from the *away* architecture in the whole time span of about 50 hours following the start of the activation of the PG device with conductive heat transfer from a 100 Ω resistor. (a) Voltage difference $\Delta V(t)$. (b) Temperature difference $\Delta T(t)$. Temperatures $T_{hot}(t)$ (c) and $T_{cold}(t)$ (d) of the activated and non-activated faces, respectively, of the PG device. The PG device was horizontally fixed on the sample holders in these measurements and was finished with a layer of pink-colored gaffer tape on the AlO plate. The unit for time is the hour ([h]).
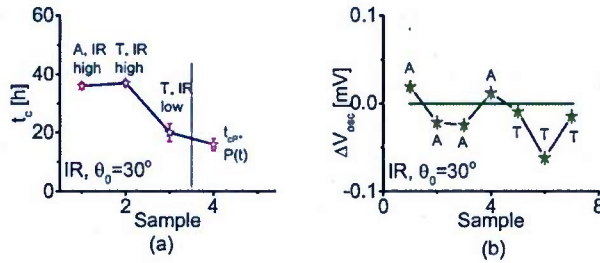

Figure A4. (a) Averages of the critical time (t_c) and (b) amplitude (ΔV_{osc}) of the hyperbolic instability detected in the time span of about 50 hours following the start of the illumination of the PG device with IR radiation. The data were collected performing measurements on a PG device finished with an AlO plate, described in Appendix-1, and in the *away* (A) and the *toward* (T) architectures. The PG device was positioned horizontally and at an angle of incidence $\theta_0 = 30°$ with respect to the IR radiation. The average of the higher and lower values of t_c found in the *away* and *toward* architectures are compared with the average value of t_{cP} at 16 ± 2 h for the power $P(t)$. In (b), the horizontal line separates the positive and negative ΔV_{osc}.

the layer of tape facing the IR radiation, the surface density $\sigma(z,t)$ refers to the charges in the AlO plate or in the tape. The results, summarized in **Figure A4**, report the average values of the critical time (t_c) and amplitudes (ΔV_{osc}) of the revealed hyperbolic instabilities. We found a correlation neither between the values of t_c in **Figure A4(a)** and the signs of ΔV_{osc} in **Figure A4(b)**, nor between these quantities and the *away* or *toward* architectures. However, by observing **Figure A4(a)**, we found that t_c is typically located around 36 ± 1 h, which is about twice the magnitude of t_{cP} at 16 ± 2 h for the sinusoidal instability in $P(t)$ of the IR source reported in **Table 2**. In addition, we noted lower values for t_c in **Figure A4(a)** located around 20 ± 3 h, *i.e.* in the neighborhood of t_{cP}. These observations highlight the correlations existing between the instabilities in $P(t)$ and $\Delta V(t)$ as already discussed in Section 3(e). Furthermore, in **Figure A4(b)** we noted randomness in the sign of ΔV_{osc}, which we attribute to the loss of correlation between the phase of $P(t)$ and $\sigma(z,t)$, and then between $\sigma(z,t)$ and $\Delta V(t)$. We predicted the loss of phase relationship in Section 3(b).

We summarize the findings in **Figure A4** as follows: the hyperbolic instability in $\Delta V(t)$ is a common phenomenon, which is linked with the sinusoidal instability in the power $P(t)$ of the IR radiation.